Chapter 12
Peridynamic Thermal Diffusion

The peridynamic (PD) theory can be applied to other physical fields such as thermal diffusion, neutronic diffusion, vacancy diffusion, and electrical potential distribution. This paves the way for fully coupling various field equations and deformation within the framework of peridynamics using the same computational domain.

12.1 Basics

In heat conduction, the thermal energy is transported through phonons, lattice vibrations, and electrons. Usually, electrons are the vehicles through which thermal energy is transported in metals while phonons are the heat carriers in insulators and semiconductors. This process of thermal energy transfer is inherently nonlocal because the carriers arrive at one point, having brought thermal energy from another. The mean free path of the heat carriers is the average distance a carrier travels before its excess energy is lost. As the heat carriers' mean free path becomes comparable to the characteristic lengths, the nonlocality needs to be taken into account in the continuum model.

Although heat transfer and temperature are closely related, they are of a different nature. Temperature has only a magnitude, and heat transfer has a direction as well as a magnitude. Temperature difference between the material points in a medium is the driving force for any type of heat transfer. In a body, heat flows in the direction of decreasing temperature. Physical experiments show that the rate of heat flow is proportional to the gradient of the temperature, and the proportionality constant, k, represents thermal conductivity of the material. This observation, referred to as Fourier's law of heat conduction, is expressed as

$$\mathbf{q} = -k\,\nabla\Theta, \tag{12.1}$$

where $\mathbf{q}$ is the heat flux vector, k is the thermal conductivity, and $\nabla\Theta$ is the gradient of temperature. The minus sign ensures that heat flows in the direction of decreasing

E. Madenci and E. Oterkus, *Peridynamic Theory and Its Applications*,
DOI 10.1007/978-1-4614-8465-3_12,

temperature. The rate of heat entering through the bounding surface, $\mathcal{S}$, with unit normal, $\mathbf{n}$, can be obtained from

$$\dot{Q} = -\int_{\mathcal{S}} \mathbf{q}.\mathbf{n} d\mathcal{S}, \tag{12.2}$$

in which the minus sign ensures that heat flow is into the body. If the rate of heat, $\dot{Q}$, is positive, it indicates a heat gain. Otherwise, it is a heat loss. This formulation employing Fourier's law as the local constitutive relation has been used successfully to model macroscale heat conduction.

12.2 Nonlocal Thermal Diffusion

Nonlocality often becomes important at low temperatures, as exhibited in cryogenics systems, since the heat carriers have a longer mean free path at lower temperatures. It has been found that nonlocality should also be accounted for in problems in which the temperature gradients are steep. This is because the penetration depth, the length characterizing the temperature gradient, becomes short, even becoming the same order of magnitude as the mean free path of the carrier. In such instances, it is necessary to consider the nonlocality of the heat transport in a continuum model. With the miniaturization of devices, the short geometric length scales also necessitated the inclusion of nonlocal effects in microscale and nanoscale models (Tien and Chen 1994).

Several nonlocal heat conduction theories have been proposed in the last few decades. In the early 1980s, Luciani et al. (1983) developed a nonlocal theory to better represent electron heat transport down a steep temperature gradient by introducing a nonlocal expression for the heat flux. The nonlocal model was in better agreement with probabilistic simulations (Fokker-Planck simulations) than the local models. Later, Mahan and Claro (1988) proposed a nonlocal relation between the heat current, determined from Boltzmann's equation, and the temperature gradient. In the 1990s, Sobolev (1994) introduced a model in which both space and time nonlocality are taken into account in the strong form, i.e., integral form, of the energy balance, Gibbs, and entropy balance equations. Lebon and Grmela (1996), proposed a weakly nonlocal model (weakly nonlocal models are typically based on gradient formulations). The model was based on nonequilibrium thermodynamics, for which an extra variable is added to the basic state variables to account for nonlocality. Subsequently, they extended their model to include nonlinearity (Grmela and Lebon 1998). More recently, the development of nonlocal heat conduction equations has been motivated by the miniaturization of devices. A number of researchers have put forth nonlocal models with the objective of capturing heat transport in microscale and nanoscale devices. One example of this is the ballistic-diffusive heat equation by Chen (2002), which was derived

from the Boltzmann's equation, and it accounts for nonlocality in heat transport. Another example is by Alvarez and Jou (2007). They developed their model by including nonlocal (and memory/lag) effects in irreversible thermodynamics. Tzou and Guo (2010) constructed their model by incorporating a nonlocal (and lag) term into the Fourier law.

An area of interest is determining the temperature field in the presence of emerging discontinuities. One class of problems that contains a discontinuity is the heat transfer process that involves phase changes such as solidification and melting (Özişik 1980). This process is commonly referred to as the Stefan problem, and there are a number of technologically important problems that involve heat transfer with phase change. Examples of these include ablation of space vehicles during reentry and casting of metals. Another heat conduction problem with an emerging discontinuity is the rewetting problem from the nuclear industry. Rewetting in a nuclear reactor is employed to restore temperatures to a safe range following accidental dry-out or loss of coolant. Emergency cooling is introduced to the system via an upward moving water front or by spraying from the top of the reactor (Duffey and Porthous 1973; Dorfman 2004). A moving discontinuity occurs in the heat-generating solid at the quench front due to the sudden change in the heat transfer condition at the solid surface.

A peridynamic approach to heat conduction is advantageous because it not only accounts for nonlocality but it also allows for the determination of the temperature field in spite of discontinuities. The peridynamic heat conduction is a continuum model; it is not a discrete model. As such, the phonon and electron motions are not explicitly modeled. Initial successful attempts have recently been made to develop heat conduction equations in the peridynamic framework. Gerstle et al. (2008) developed a PD model for electromigration that accounts for heat conduction in a one-dimensional body. Additionally, Bobaru and Duangpanya (2010, 2012) introduced a multi-dimensional peridynamic heat conduction equation, and considered domains with discontinuities such as insulated cracks. Both studies adopted the bond-based PD approach. Later, Agwai (2011) derived a state-based PD heat conduction equation, which is described in the subsequent section.

12.3 State-Based Peridynamic Thermal Diffusion

Within the peridynamic framework, the interaction between material points is nonlocal. For thermal diffusion, the nonlocal interaction between material points is due to the exchange of heat energy. Therefore, a material point will exchange heat with points within its neighborhood defined by the horizon. In the Lagrangian formalism, the governing heat conduction equation corresponds to the Euler-Lagrange equation. The Euler-Lagrange equation based on the Lagrangian, L, is given in the following form (Moiseiwitsch 2004):

$$\frac{d}{dt}\left(\frac{\partial L}{\partial \dot{\Theta}}\right) - \frac{\partial L}{\partial \Theta} = 0, \tag{12.3a}$$

with

$$L = \int_V \mathfrak{L} dV, \tag{12.3b}$$

in which Θ is the temperature and $\mathfrak{L}$ is the Lagrangian density. The Lagrangian density of a peridynamic material point can be defined as

$$\mathfrak{L} = Z + \rho \widehat{s} \Theta, \tag{12.4}$$

where Z is thermal potential and is a function of all the temperatures of the points with which $\mathbf{x}$ interacts, ρ is the density, and $\widehat{s}$ is the heat source per unit mass, which includes the rate of heat generation per unit volume and the internal energy storage. There is a thermal potential associated with each material point, and the term $Z_{(i)}$ represents the thermal potential of material point $\mathbf{x}_{(i)}$. The microthermal potential, $z_{(i)(j)}$, is the thermal potential due to the interaction (exchange of heat energy) between material points $\mathbf{x}_{(i)}$ and $\mathbf{x}_{(j)}$. The microthermal potential is related to heat energy exchange, which depends on the temperature difference between the material points. Therefore, the microthermal potential is dependent on the temperature difference between pairs of material points. More specifically, the microthermal potential, $z_{(i)(j)}$, depends on the temperature difference between point i and all other material points that interact with point $\mathbf{x}_{(i)}$. Note that the microthermal potential $z_{(j)(i)} \neq z_{(i)(j)}$, as $z_{(j)(i)}$ depends on the state of material points that interact with material point $\mathbf{x}_{(j)}$. The microthermal potential is denoted as follows:

$$z_{(i)(j)} = z_{(i)(j)}\left(\Theta_{(1^i)} - \Theta_{(i)},\ \Theta_{(2^i)} - \Theta_{(i)}, \cdots\right), \tag{12.5a}$$

$$z_{(j)(i)} = z_{(j)(i)}\left(\Theta_{(1^j)} - \Theta_{(j)},\ \Theta_{(2^j)} - \Theta_{(j)}, \cdots\right), \tag{12.5b}$$

where $\Theta_{(i)}$ is the temperature at point $\mathbf{x}_{(i)}$, $\Theta_{(1^i)}$ is the temperature of the first material point that interacts with point $\mathbf{x}_{(i)}$, and, similarly, $\Theta_{(j)}$ is the temperature at point $\mathbf{x}_{(j)}$ while $\Theta_{(1^j)}$ is the temperature of the first material point that interacts with point $\mathbf{x}_{(j)}$.

The thermal potential of point $\mathbf{x}_{(i)}$, $Z_{(i)}$ is defined as

$$\begin{aligned} Z_{(i)} = \frac{1}{2}\sum_{j=1}^{\infty}\frac{1}{2}\big(&z_{(i)(j)}\left(\Theta_{(1^i)} - \Theta_{(i)},\ \Theta_{(2^i)} - \Theta_{(i)}, \cdots\right) \\ &+ z_{(j)(i)}\left(\Theta_{(1^j)} - \Theta_{(j)},\ \Theta_{(2^j)} - \Theta_{(j)}, \cdots\right)\big) V_{(j)}, \end{aligned} \tag{12.6}$$

where $V_{(j)}$ is the volume associated with material point $\mathbf{x}_{(j)}$. Basically, this equation indicates that the thermal potential at a point is the summation over all the microthermal potential associated with that point. The microthermal potential and therefore thermal potential are both functions of temperature. The Euler-Lagrange equation, Eq. 12.3a, for material point $\mathbf{x}_{(k)}$ becomes

$$\frac{d}{dt}\left(\frac{\partial L}{\partial \dot{\Theta}_{(k)}}\right) - \frac{\partial L}{\partial \Theta_{(k)}} = 0, \tag{12.7a}$$

in which

$$L = \sum_{i=1}^{\infty} \mathfrak{L}_{(i)} V_{(i)}, \tag{12.7b}$$

with

$$\mathfrak{L}_{(i)} = Z_{(i)} + \rho \widehat{s}_{(i)} \Theta_{(i)}. \tag{12.7c}$$

Consequently, invoking Eq. 12.6 into Eq. 12.7b results in the Lagrangian function as

$$\begin{aligned} L = \sum_{i=1}^{\infty} \Bigg\{ \frac{1}{2} \sum_{j=1}^{\infty} \frac{1}{2} \Bigg[& z_{(i)(j)}\left(\Theta_{(1^i)} - \Theta_{(i)}, \Theta_{(2^i)} - \Theta_{(i)}, \cdots\right) \\ & + z_{(j)(i)}\left(\Theta_{(1^j)} - \Theta_{(j)}, \Theta_{(2^j)} - \Theta_{(j)}, \cdots\right) \Bigg] V_{(j)} \\ & + \rho \widehat{s}_{(i)} \Theta_{(i)} \Bigg\} V_{(i)}, \end{aligned} \tag{12.8a}$$

which can be written in an expanded form by showing only the terms associated with the material point $\mathbf{x}_{(k)}$:

$$\begin{aligned} L = \cdots & \frac{1}{2} \sum_{j=1}^{\infty} \Bigg\{ \frac{1}{2} \Big[z_{(k)(j)}\left(\Theta_{(1^k)} - \Theta_{(k)},\ \Theta_{(2^k)} - \Theta_{(k)}, \cdots\right) \\ & + z_{(j)(k)}\left(\Theta_{(1^j)} - \Theta_{(j)},\ \Theta_{(2^j)} - \Theta_{(j)}, \cdots\right) \Big] V_{(j)} \Bigg\} V_{(k)} \cdots \\ & \cdots + \frac{1}{2} \sum_{i=1}^{\infty} \Bigg\{ \frac{1}{2} \Big[z_{(i)(k)}\left(\Theta_{(1^i)} - \Theta_{(i)},\ \Theta_{(2^i)} - \Theta_{(i)}, \cdots\right) \\ & + z_{(k)(i)}\left(\Theta_{(1^k)} - \Theta_{(k)},\ \Theta_{(2^k)} - \Theta_{(k)}, \cdots\right) \Big] V_{(k)} \Bigg\} V_{(i)} \cdots \\ & \cdots + \left(\rho \widehat{s}_{(k)} \Theta_{(k)}\right) V_{(k)} \cdots \end{aligned} \tag{12.8b}$$

or

$$L = \cdots \sum_{j=1}^{\infty} \left\{ \frac{1}{2} \left[z_{(k)(j)} \left(\Theta_{(1^k)} - \Theta_{(k)},\ \Theta_{(2^k)} - \Theta_{(k)}, \cdots \right) \right.\right. \\ \left.\left. + z_{(j)(k)} \left(\Theta_{(1^j)} - \Theta_{(j)},\ \Theta_{(2^j)} - \Theta_{(j)}, \cdots \right) \right] V_{(j)} \right\} V_{(k)} \cdots \\ \cdots + \left(\rho \widehat{s}_{(k)} \Theta_{(k)} \right) V_{(k)} \cdots . \tag{12.8c}$$

With this representation, the Euler-Lagrange equation, Eq. 12.7a, becomes

$$\left(\sum_{j=1}^{\infty} \frac{1}{2} \left(\sum_{i=1}^{\infty} \frac{\partial z_{(k)(i)}}{\partial \left(\Theta_{(j)} - \Theta_{(k)} \right)} V_{(i)} \right) \frac{\partial \left(\Theta_{(j)} - \Theta_{(k)} \right)}{\partial \Theta_{(k)}} \right. \\ \left. + \sum_{j=1}^{\infty} \frac{1}{2} \left(\sum_{i=1}^{\infty} \frac{\partial z_{(i)(k)}}{\partial \left(\Theta_{(k)} - \Theta_{(j)} \right)} V_{(i)} \right) \frac{\partial \left(\Theta_{(k)} - \Theta_{(j)} \right)}{\partial \Theta_{(k)}} V_{(j)} \right) V_{(k)} + \rho \widehat{s}_{(k)} V_{(k)} = 0 \tag{12.9a}$$

or

$$- \sum_{j=1}^{\infty} \frac{1}{2} \left(\sum_{i=1}^{\infty} \frac{\partial z_{(k)(i)}}{\partial \left(\Theta_{(j)} - \Theta_{(k)} \right)} V_{(i)} \right) + \sum_{j=1}^{\infty} \left(\sum_{i=1}^{\infty} \frac{\partial z_{(i)(k)}}{\partial \left(\Theta_{(k)} - \Theta_{(j)} \right)} V_{(i)} \right) + \rho \widehat{s}_{(k)} = 0, \tag{12.9b}$$

in which the terms $\sum_{i=1}^{\infty} V_{(i)} \partial z_{(k)(i)} / \partial \left(\Theta_{(j)} - \Theta_{(k)} \right)$ and $\sum_{i=1}^{\infty} V_{(i)} \partial z_{(i)(k)} / \partial \left(\Theta_{(k)} - \Theta_{(j)} \right)$ can be thought of as the heat flow density from material point $\mathbf{x}_{(j)}$ to material point $\mathbf{x}_{(k)}$ and the heat flow density from material point $\mathbf{x}_{(k)}$ to $\mathbf{x}_{(j)}$, respectively. Based on this interpretation, $\mathcal{H}_{(k)(j)}$ and $\mathcal{H}_{(j)(k)}$ are introduced and defined as

$$\mathcal{H}_{(k)(j)} = \frac{1}{2} \frac{1}{V_{(j)}} \left(\sum_{i=1}^{\infty} \frac{\partial z_{(k)(i)}}{\partial \left(\Theta_{(j)} - \Theta_{(k)} \right)} V_{(i)} \right) \quad \text{and} \quad \mathcal{H}_{(j)(k)} = \frac{1}{2} \frac{1}{V_{(j)}} \left(\sum_{i=1}^{\infty} \frac{\partial z_{(i)(k)}}{\partial \left(\Theta_{(k)} - \Theta_{(j)} \right)} V_{(i)} \right). \tag{12.10}$$

Using these definitions allows Eq. 12.9b to be rewritten as follows:

$$\sum_{j=1}^{\infty} \left(-\mathcal{H}_{(k)(j)} + \mathcal{H}_{(j)(k)} \right) V_{(j)} + \rho \widehat{s}_{(k)} = 0. \tag{12.11}$$

A PD state can be thought of as an infinite dimensional array that contains certain information about all the interactions associated with a particular material point. All of the heat flow density associated with each interaction assembled in an infinite-dimensional array is referred to as the heat flow *scalar* state, $\underline{h}(\mathbf{x}, t)$, where t is the time. The assembled heat flow state for material points $\mathbf{x}_{(k)}$ and $\mathbf{x}_{(j)}$ may be represented as

$$\underline{h}\big(\mathbf{x}_{(k)},t\big)=\left\{\begin{array}{c}\vdots\\ \mathcal{H}_{(k)(j)}\\ \vdots\end{array}\right\}\quad\text{and}\quad\underline{h}\big(\mathbf{x}_{(j)},t\big)=\left\{\begin{array}{c}\vdots\\ \mathcal{H}_{(j)(k)}\\ \vdots\end{array}\right\}. \tag{12.12}$$

The heat flow state associates each pair of interacting material points with a heat flow density, and enables the expressions for heat flow densities $\mathcal{H}_{(k)(j)}$ and $\mathcal{H}_{(j)(k)}$ as

$$\mathcal{H}_{(k)(j)}=\underline{h}\big(\mathbf{x}_{(k)},t\big)\left\langle\mathbf{x}_{(j)}-\mathbf{x}_{(k)}\right\rangle\quad\text{and}\quad\mathcal{H}_{(j)(k)}=\underline{h}\big(\mathbf{x}_{(j)},t\big)\left\langle\mathbf{x}_{(k)}-\mathbf{x}_{(j)}\right\rangle, \tag{12.13}$$

where the angled brackets include the interacting material points. The microthermal potentials may also be assembled in a state, which is called the microthermal potential *scalar* state, $\underline{z}(\mathbf{x},t)$, permitting the following representation:

$$z_{(k)(j)}=\underline{z}\big(\mathbf{x}_{(k)},t\big)\left\langle\mathbf{x}_{(j)}-\mathbf{x}_{(k)}\right\rangle\quad\text{and}\quad z_{(j)(k)}=\underline{z}\big(\mathbf{x}_{(j)},t\big)\left\langle\mathbf{x}_{(k)}-\mathbf{x}_{(j)}\right\rangle. \tag{12.14}$$

Applying the state notation, Eq. 12.11 can be rewritten as

$$\sum_{j=1}^{\infty}\Big(\underline{h}\big(\mathbf{x}_{(k)},t\big)\left\langle\mathbf{x}_{(j)}-\mathbf{x}_{(k)}\right\rangle-\underline{h}\big(\mathbf{x}_{(j)},t\big)\left\langle\mathbf{x}_{(k)}-\mathbf{x}_{(j)}\right\rangle\Big)\,V_{(j)}-\rho\widehat{s}_{(k)}=0. \tag{12.15}$$

Transforming the summation to integration over the material points within the horizon as given by

$$\sum_{j=1}^{\infty}(\cdot)\,V_{(j)}\rightarrow\int_{H}(\cdot)\,dV_{\mathbf{x}'} \tag{12.16}$$

permits Eq. 12.15 to be recast as

$$\int_{H}(\underline{h}(\mathbf{x},t)\langle\mathbf{x}'-\mathbf{x}\rangle-\underline{h}(\mathbf{x}',t)\langle\mathbf{x}-\mathbf{x}'\rangle)dV_{\mathbf{x}'}-\rho\widehat{s}=0, \tag{12.17}$$

where $\underline{h}(\mathbf{x},t)\langle\mathbf{x}'-\mathbf{x}\rangle=0$ for $\mathbf{x}'\notin H$, and the domain of integration, H, is defined by the horizon of the material point, $\mathbf{x}$, that interacts with other material points in its own family.

For convenience, the following notation is adopted:

$$\underline{h}(\mathbf{x},t)=\underline{h},\qquad\underline{h}(\mathbf{x}',t)=\underline{h}'. \tag{12.18}$$

Also, the temperature *scalar* state, $\underline{\tau}$, is defined as

$$\underline{\tau}(\mathbf{x},t)\langle\mathbf{x}'-\mathbf{x}\rangle=\Theta(\mathbf{x}',t)-\Theta(\mathbf{x},t). \tag{12.19}$$

The temperature state simply contains the temperature difference associated with each interaction of a particular material point. Since, the microthermal potential is dependent on the temperature difference of all the interactions associated with the material point, it may be written as a function of the temperature state

$$\underline{z} = \underline{z}(\underline{\tau}). \tag{12.20}$$

Therefore, the heat flow state can also be written as a function of the temperature state

$$\underline{h} = \underline{h}(\underline{\tau}). \tag{12.21}$$

As outlined by Bathe (1996), the heat conduction equation should explicitly include the rate at which heat energy is stored when the heat flow changes over a short period of time. This rate of internal energy storage density, $\dot{\varepsilon}_s$, is a negative energy source and is given by

$$\dot{\varepsilon}_s = c_v \frac{\partial \Theta}{\partial t}, \tag{12.22}$$

for which c_v is the specific heat capacity.

Therefore, the source term in Eq. 12.15 is then replaced by $\widehat{s} = \dot{\varepsilon}_s - s_b$, where s_b is the heat source due to volumetric heat generation per unit mass. Invoking Eq. 12.22 into Eq. 12.15 leads to the transient form of the state-based peridynamic thermal diffusion equation

$$\rho c_v \dot{\Theta}(\mathbf{x}, t) = \int_H \underline{h}(\mathbf{x}, t)\langle \mathbf{x}' - \mathbf{x} \rangle - \underline{h}(\mathbf{x}', t)\langle \mathbf{x} - \mathbf{x}' \rangle dV' + h_s(\mathbf{x}, t), \tag{12.23}$$

in which $h_s(\mathbf{x}, t) = \rho s_b(\mathbf{x}, t)$ is the heat source due to volumetric heat generation. The resulting equation is an integro-differential equation in time and space. It contains differentiation with respect to time, and integration in the spatial domain. It does not contain any spatial derivatives of temperature; thus, the PD thermal equation is valid everywhere whether or not discontinuities exist in the domain. Construction of its solution involves time and spatial integrations while being subject to conditions on the boundary of the domain, $\mathcal{R}$, and initial conditions.

12.4 Relationship Between Heat Flux and Peridynamic Heat Flow States

The heat flow *scalar* state, $\underline{h}$, contains the heat flow densities associated with all the interactions. The heat flow density, $\underline{h}(\mathbf{x},t)\langle \mathbf{x}'-\mathbf{x}\rangle$, has units of heat flow rate (rate of heat energy change) per volume squared. The integral in Eq. 12.23

$$\int_H \underline{h}(\mathbf{x},t)\langle \mathbf{x}'-\mathbf{x}\rangle - \underline{h}(\mathbf{x}',t)\langle \mathbf{x}-\mathbf{x}'\rangle dV' \tag{12.24}$$

is similar to the divergence of heat flux, $\nabla\cdot\mathbf{q}$, and it has units of heat flow rate per volume. Therefore, the peridynamic heat flow state can be related to the heat flux, $\mathbf{q}$.

Multiplying the PD heat conduction equation, Eq. 12.23, by a temperature variation of $\Delta\Theta$ and integrating over the entire domain results in

$$\begin{aligned}\int_V \rho c_v \dot{\Theta}\Delta\Theta dV = &\int_V\int_H [\underline{h}(\mathbf{x},t)\langle \mathbf{x}'-\mathbf{x}\rangle - \underline{h}(\mathbf{x}',t)\langle \mathbf{x}-\mathbf{x}'\rangle]\Delta\Theta dV' dV \\ &+ \int_V h_s(\mathbf{x},t)\Delta\Theta dV t\ .\end{aligned} \tag{12.25}$$

Moving the last term on the right-hand side of Eq. 12.25, the heat generation term, to the left-hand side, and changing the integration from H to V due to the fact that

$$\underline{h}(\mathbf{x},t)\langle \mathbf{x}'-\mathbf{x}\rangle = \underline{h}(\mathbf{x}',t)\langle \mathbf{x}-\mathbf{x}'\rangle = 0 \text{ for } \mathbf{x}'\notin H, \tag{12.26}$$

leads to the following form of the equation:

$$\int_V \left[\rho c_v\dot{\Theta} - h_s(\mathbf{x},t)\right]\Delta\Theta dV = \int_V\int_V [\underline{h}(\mathbf{x},t)\langle \mathbf{x}'-\mathbf{x}\rangle \quad -\underline{h}(\mathbf{x}',t)\langle \mathbf{x}-\mathbf{x}'\rangle]\Delta\Theta dV' dV\ . \tag{12.27}$$

If the parameters $\mathbf{x}$ and $\mathbf{x}'$ in the second integral on the right-hand side of Eq. 12.27 are exchanged, the second integral becomes

$$\int_V\int_V \underline{h}(\mathbf{x}',t)\langle \mathbf{x}-\mathbf{x}'\rangle\Delta\Theta dV' dV = \int_V\int_V \underline{h}(\mathbf{x},t)\langle \mathbf{x}'-\mathbf{x}\rangle\Delta\Theta' dV dV'. \tag{12.28}$$

Substituting from Eq. 12.28 into Eq. 12.27, leads to

$$\int_V \left[\rho c_v \dot{\Theta} - h_s(\mathbf{x},t)\right]\Delta\Theta dV = \int_V \int_V \underline{h}(\mathbf{x},t)\langle \mathbf{x}' - \mathbf{x}\rangle(\Delta\Theta - \Delta\Theta')dV'dV. \tag{12.29}$$

Invoking the variation of the temperature *scalar* state, $\Delta\underline{\tau}$, from Eq. 12.19 into Eq. 12.29 results in

$$\int_V \left[\rho c_v \dot{\Theta} - h_s(\mathbf{x},t)\right]\Delta\Theta dV = \int_V \Delta Z dV, \tag{12.30}$$

where ΔZ corresponds to the variation of the PD thermal potential at $\mathbf{x}$ due to its interactions with all other material points:

$$\Delta Z = -\int_V (\underline{h}(\mathbf{x},t)\langle \mathbf{x}' - \mathbf{x}\rangle)(\Delta\underline{\tau}\langle \mathbf{x}' - \mathbf{x}\rangle)dV'. \tag{12.31}$$

Considering only the material points within the horizon, Eq. 12.31 can be rewritten as

$$\Delta Z = -\int_H (\underline{h}(\mathbf{x},t)\langle \mathbf{x}' - \mathbf{x}\rangle)(\Delta\underline{\tau}\langle \mathbf{x}' - \mathbf{x}\rangle)dV'. \tag{12.32}$$

Based on the classical formulation, the corresponding variation of thermal potential can be written as

$$\Delta\hat{Z}(\bar{\mathbf{G}}) = \frac{1}{2}\left(\Delta\bar{\mathbf{G}}\cdot k\,\bar{\mathbf{G}} + \bar{\mathbf{G}}\cdot k\Delta\,\bar{\mathbf{G}}\right) = k\bar{\mathbf{G}}\cdot\Delta\,\bar{\mathbf{G}}, \tag{12.33a}$$

with $\hat{Z}(\bar{\mathbf{G}})$ given by

$$\hat{Z}(\bar{\mathbf{G}}) = \frac{1}{2}\bar{\mathbf{G}}\cdot k\,\bar{\mathbf{G}}, \tag{12.33b}$$

where k is the thermal conductivity and $\bar{\mathbf{G}} = \nabla\Theta$. After invoking the Fourier relation, $\mathbf{q} = -k\,\bar{\mathbf{G}}$, the variation of classical thermal potential can be rewritten as

$$\Delta\hat{Z}(\bar{\mathbf{G}}) = -\mathbf{q}\cdot\Delta\bar{\mathbf{G}}. \tag{12.34}$$

By applying the definition of scalar reduction given in the Appendix, the temperature gradient can be approximated as

$$\Delta\bar{\mathbf{G}} = \frac{1}{m}\Delta\underline{\tau} * \underline{\mathbf{X}} = \frac{1}{m}\int_H \underline{w}\langle \mathbf{x}' - \mathbf{x}\rangle\Delta\underline{\tau}\langle \mathbf{x}' - \mathbf{x}\rangle \otimes \underline{\mathbf{X}}\langle \mathbf{x}' - \mathbf{x}\rangle dV', \tag{12.35}$$

in which $\Delta\underline{\tau}$ is a *scalar* state, thus not requiring the dyadic, $\otimes$, operation. It reduces to

$$\Delta\bar{\mathbf{G}} = \frac{1}{m}\int_H \underline{w}\langle \mathbf{x}'-\mathbf{x}\rangle \underline{\mathbf{X}}\langle \mathbf{x}'-\mathbf{x}\rangle \Delta\underline{\tau}\langle \mathbf{x}'-\mathbf{x}\rangle dV', \tag{12.36}$$

where $\underline{w}$ is a scalar state representing the influence function, and m is the scalar weighted volume defined in the Appendix.

Its substitution into Eq. 12.34 leads to the following:

$$\Delta\hat{Z} = -\frac{1}{m}\int_H \mathbf{q}^T \underline{w}\langle \mathbf{x}'-\mathbf{x}\rangle \underline{\mathbf{X}}\langle \mathbf{x}'-\mathbf{x}\rangle \Delta\underline{\tau}\langle \mathbf{x}'-\mathbf{x}\rangle dV'. \tag{12.37}$$

Assuming that the variation of the PD thermal potential, ΔZ, and classical thermal potential, $\Delta\hat{Z}$, are equal, $\Delta Z = \Delta\hat{Z}$, and comparing Eq. 12.31 to Eq. 12.37, it follows that

$$\underline{h}(\mathbf{x},t)\langle \mathbf{x}'-\mathbf{x}\rangle = \frac{1}{m}\mathbf{q}^T \underline{w}\langle \mathbf{x}'-\mathbf{x}\rangle \underline{\mathbf{X}}\langle \mathbf{x}'-\mathbf{x}\rangle, \tag{12.38}$$

and this expression relates the heat flow state to the heat flux.

12.5 Initial and Boundary Conditions

The PD thermal equation does not contain any spatial derivatives; thus, boundary conditions are, in general, not necessary for the solution of an integro-differential equation. However, such conditions on temperature can be imposed in a "fictitious material layer" along the boundary of a nonzero volume.

Heat flux does not directly appear in the PD thermal diffusion equation. Therefore, the application of heat flux is also different from that of the classical heat conduction theory. The difference can be illustrated by considering a region, Ω, that is in thermal equilibrium. If this region is fictitiously divided into two domains, Ω^- and Ω^+ as shown in Fig. 12.1, there must be rates of heat flow $\dot{Q}^+$ and $\dot{Q}^-$ entering through the cross-sectional surfaces, $\partial\Omega$, of domain Ω^+ and Ω^-.

According to classical heat conduction theory, the heat flow rates, $\dot{Q}^+$ and $\dot{Q}^-$, can be determined by integrating the normal component of the heat flux over the cross-sectional area, $\partial\Omega$, of domains Ω^+ and Ω^- as

$$\dot{Q}^+ = -\int_{\partial\Omega} \mathbf{q}^+ \cdot \mathbf{n}^+ d\mathcal{S} \tag{12.39a}$$

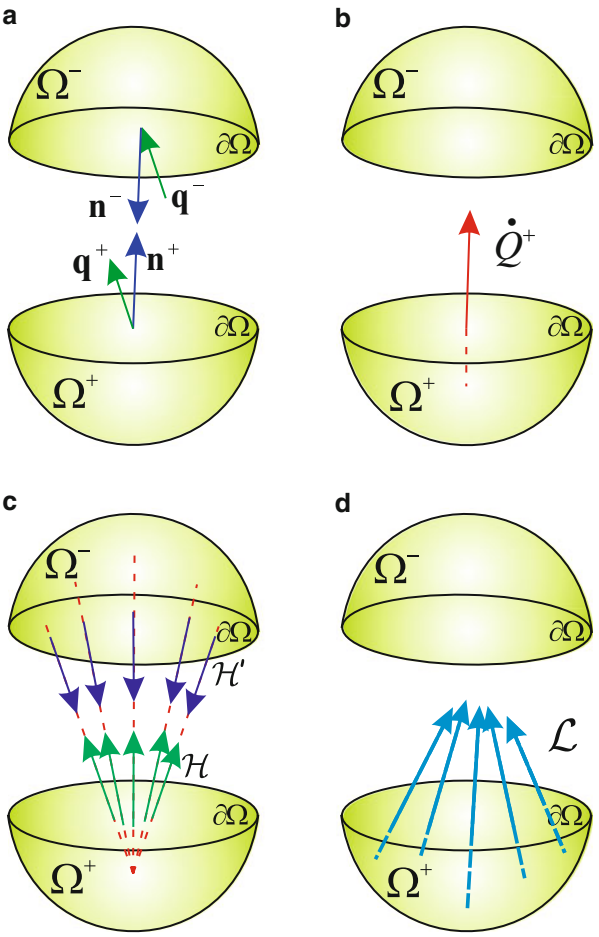

Fig. 12.1 Boundary conditions: (**a**) heat fluxes through the cross-sectional area, (**b**) heat flow rate in classical heat conduction theory, (**c**) heat flow density of a material point in domain Ω^+ with other material points in domain Ω^-, (**d**) heat flux density from domain Ω^+ due to domain Ω^-

and

$$\dot{Q}^- = -\int_{\partial\Omega} \mathbf{q}^- \cdot \mathbf{n}^- d\mathcal{S}, \tag{12.39b}$$

in which $\mathbf{q}^+$ and $\mathbf{q}^-$ are the heat fluxes across the surfaces with unit normal vectors, $\mathbf{n}^+$ and $\mathbf{n}^-$, of domains Ω^+ and Ω^-, as shown in Fig. 12.1a, b.

In the case of the PD theory, the material points located in domain Ω^+ interact with the other material points in domain Ω^- (Fig. 12.1c). Thus, the heat flow rate, $\dot{Q}^+$, can be computed by volume integration of the heat flux densities (Fig. 12.1d) over domain Ω^+ as

$$\dot{Q}^{+} = \int_{\Omega^{+}} \mathcal{L}(\mathbf{x}) dV, \tag{12.40a}$$

in which $\mathcal{L}(\mathbf{x})$, acting on a material point in domain Ω^{+}, is determined by

$$\mathcal{L}(x) = \int_{\Omega^{-}} [\underline{h}(\mathbf{x}, t)\langle \mathbf{x}' - \mathbf{x} \rangle - \underline{h}(\mathbf{x}', t)\langle \mathbf{x} - \mathbf{x}' \rangle] dV \,. \tag{12.40b}$$

Note that if the volume Ω^{-} is void, the volume integration in Eq. 12.40b vanishes. Hence, the heat flux cannot be applied as a boundary condition since its volume integrations result in a zero value. Therefore, the heat flux can be applied as rate of volumetric heat generation in a "real material layer" along the boundary of a nonzero volume.

12.5.1 Initial Conditions

Time integration requires the application of initial temperature values at each material point in the domain, $\mathcal{R}$, as shown in Fig. 12.2, and they can be specified as

$$\Theta(\mathbf{x}, t = 0) = \Theta^{*}(\mathbf{x}). \tag{12.41}$$

12.5.2 Boundary Conditions

Boundary conditions can be imposed as temperature, heat flux, convection, and radiation. As shown in Fig. 12.2, the prescribed boundary temperature is imposed in a layer of a fictitious region, $\mathcal{R}_t$, along the boundary of the actual material surface, $\mathcal{S}_t$, of the actual material region, $\mathcal{R}$. Based on numerical experiments, the extent of the fictitious boundary layer must be equal to the horizon, δ, in order to ensure that the prescribed temperatures are sufficiently reflected in the actual material region. The prescribed heat flux, convection, and radiation are imposed in boundary layer regions, $\mathcal{R}_f$, $\mathcal{R}_c$, and $\mathcal{R}_r$, respectively, with depth, Δ, along the boundary of the material region, $\mathcal{R}$, as shown in Fig. 12.2.

12.5.2.1 Temperature

As shown in Fig. 12.3a, the prescribed boundary temperature, $\Theta^{*}(\mathbf{x}^{*}, t)$, can be imposed in a layer of a fictitious region, $\mathcal{R}_t$, along the boundary of the actual material surface, $\mathcal{S}_t$, as

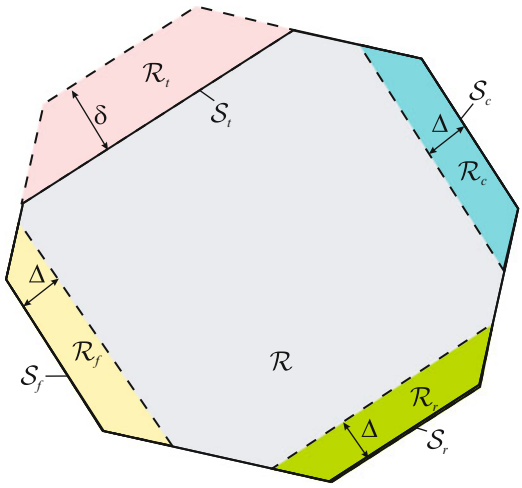

Fig. 12.2 Boundary layers for imposing temperature, heat flux, convection, and radiation

$$\Theta(\mathbf{y}, t+\Delta t) = 2\Theta^*(\mathbf{x}^*, t+\Delta t) - \Theta(\mathbf{z}, t), \quad \mathbf{x}^* \in \mathcal{S}_t, \quad \mathbf{y} \in \mathcal{R}_t, \quad \mathbf{z} \in \mathcal{R}, \quad (12.42)$$

in which $\mathbf{z}$ represents the position of a material point in $\mathcal{R}$, and $\mathbf{x}^*$ represents the location of a point on the surface, $\mathcal{S}_t$. Their relative position is such that the distance, $d = |\mathbf{x}^* - \mathbf{z}|$, between them is the shortest. The location of the image material point in $\mathcal{R}_t$ is obtained from $\mathbf{y} = \mathbf{z} + 2d\mathbf{n}$, with $\mathbf{n} = (\mathbf{x}^* - \mathbf{z})/|\mathbf{x}^* - \mathbf{z}|$. The implementation of the prescribed temperature boundary condition is demonstrated in Fig. 12.3b. For the case of $\Theta^*(\mathbf{x}^*, t) = 0$, this representation enforces the temperature variation in the fictitious region to become the negative mirror image of the temperature variation near the boundary surface in the actual material, as shown in Fig. 12.3c.

12.5.2.2 Heat Flux

Application of this type of boundary condition is accomplished by first calculating the rate of heat entering through the bounding surface by using Eq. 12.2, converting the heat flow rate, $\dot{Q}$, to a heat generation per unit volume, and then specifying this volumetric heat generation to collocations points in the boundary region. Assuming the cross-sectional area is constant for each material point, conversion is achieved by

$$\tilde{Q} = \frac{\dot{Q}}{V_f} = \frac{-\int_{\mathcal{S}_f} \mathbf{q}.\mathbf{n} d\mathcal{S}}{V_f} = -\frac{\mathbf{q}\cdot\mathbf{n}\,\mathcal{S}_f}{\mathcal{S}_f \Delta} = -\frac{\mathbf{q}\cdot\mathbf{n}}{\Delta}, \quad (12.43)$$

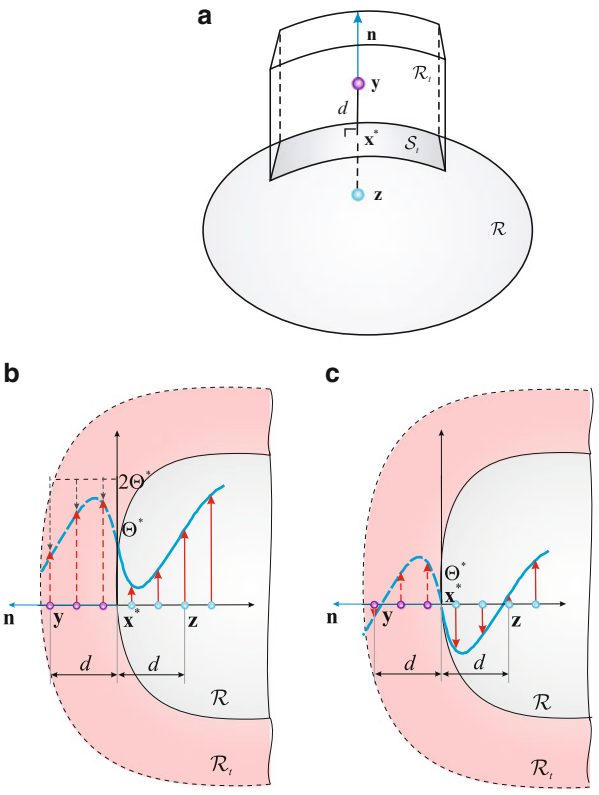

Fig. 12.3 (**a**) Material point and its image in a fictitious domain for applying, (**b**) a constant temperature condition and (**c**) a zero temperature condition

where $\tilde{Q}$ is the volumetric heat generation, $\mathbf{q}$ is the heat flux, $\mathcal{S}_f$ is the area over which the heat flux is applied, and V_f is the volume of the boundary region.

Specified flux, $\mathbf{q}^*(\mathbf{x}, t)$, over the surface $\mathcal{S}_f$, shown in Fig. 12.2, can be applied as the rate of volumetric heat generation in a boundary layer, $\mathcal{R}_f$, as

$$h_s(\mathbf{x}, t) = -\frac{1}{\Delta}\mathbf{q}^*(\mathbf{x}, t) \cdot \mathbf{n}, \text{ for } \quad \mathbf{x} \in \mathcal{R}_f. \tag{12.44}$$

If there exists no specified flux, $\mathbf{q}^*(\mathbf{x}, t) = 0$, volumetric heat generation, $\tilde{Q}$ calculated from Eq. 12.43 vanishes. Thus, the implementation of a zero flux boundary condition can be viewed as imposing a zero-valued volumetric heat generation. Alternative to this implementation, zero flux can be achieved by assigning the mirror image of the temperature values near the boundary in the actual domain to the material points in the fictitious region, as shown in Fig. 12.4.

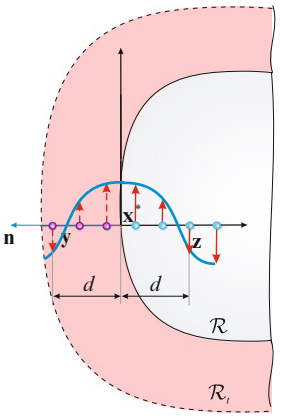

Fig. 12.4 Material point and its image in a fictitious region for imposing zero flux

12.5.2.3 Convection

Convection is a heat transfer between the surface of the body and the surrounding medium. The convection boundary condition is specified as

$$\mathbf{q}(\mathbf{x},t)\cdot\mathbf{n} = h(\Theta(\mathbf{x},t)-\Theta_\infty), \quad \text{for} \quad \mathbf{x}\in\mathcal{S}_c, \tag{12.45}$$

in which Θ_∞ is the temperature of the surrounding medium, h is the convective heat transfer coefficient, and $\Theta(\mathbf{x},t)$ is the temperature of the body on the surface, $\mathcal{S}_c$. Similar to the specified flux condition, convection can be imposed in the form of a rate of heat generation per unit volume in a boundary layer region, $\mathcal{R}_c$, as

$$h_s(\mathbf{x},t) = \frac{1}{\Delta}h(\Theta_\infty-\Theta(\mathbf{x},t)), \quad \text{for} \quad \mathbf{x}\in\mathcal{R}_c. \tag{12.46}$$

12.5.2.4 Radiation

Radiation is a heat transfer between the surface of the body and the surrounding medium. The radiation boundary condition can be written as

$$\mathbf{q}(\mathbf{x},t)\cdot\mathbf{n} = \varepsilon\sigma\left(\Theta^4(\mathbf{x},t)-\Theta_{ss}^4\right), \quad \text{for} \quad \mathbf{x}\in\mathcal{S}_r, \tag{12.47}$$

in which Θ_{ss} is the temperature of the surface surrounding the body, $\Theta(\mathbf{x},t)$ is the surface temperature of the body, σ is the Stefan-Boltzman constant, and ε is emissivity of the boundary surface. Similar to the imposition of the convection condition, radiation can also be imposed in the form of rate of heat generation per unit volume in a boundary layer region, $\mathcal{R}_r$, as

$$h_s(\mathbf{x},t)=\frac{1}{\Delta}\varepsilon\sigma\left(\Theta_{ss}^4-\Theta^4(\mathbf{x},t)\right),\quad \text{for}\quad \mathbf{x}\in\mathcal{R}_r. \tag{12.48}$$

12.6 Bond-Based Peridynamic Thermal Diffusion

If it is assumed that the heat flow density associated between two material points, $\mathbf{x}$ and $\mathbf{x}'$, is a function of the temperature difference only between these two points, then the following expression holds true:

$$\underline{h}(\mathbf{x},t)\langle\mathbf{x}'-\mathbf{x}\rangle=-\underline{h}(\mathbf{x}',t)\langle\mathbf{x}-\mathbf{x}'\rangle. \tag{12.49}$$

This leads to the specialized bond-based PD thermal diffusion. In this specialized case, the heat flow density, $f_h(\mathbf{x}',\mathbf{x},t)$, is defined as

$$f_h(\mathbf{x}',\mathbf{x},t)=\underline{h}(\mathbf{x},t)\langle\mathbf{x}'-\mathbf{x}\rangle-\underline{h}(\mathbf{x}',t)\langle\mathbf{x}-\mathbf{x}'\rangle=2\underline{h}(\mathbf{x},t)\langle\mathbf{x}'-\mathbf{x}\rangle, \tag{12.50}$$

so that the PD heat conduction equation can be written as

$$\rho c_v\dot{\Theta}(\mathbf{x},t)=\int_H f_h(\Theta',\Theta,\mathbf{x}',\mathbf{x},t)dV_{\mathbf{x}'}+\rho s_b(\mathbf{x},t). \tag{12.51}$$

The term f_h, also referred to as the thermal response function, is the heat flow density function that governs only the interaction of material point $\mathbf{x}$ with $\mathbf{x}'$. In the case of bond-based PD thermal diffusion, the pairwise interactions are independent of each other, and the heat flow between a pair of material points does not depend on the temperature difference between other pairs of material points. The thermal response function, $f_h(\mathbf{x}',\mathbf{x})$ is zero for material points outside the horizon; i.e., $|\boldsymbol{\xi}|=|\mathbf{x}'-\mathbf{x}|>\delta$.

12.7 Thermal Response Function

The pairwise heat flow density can be related to the microthermal potential through

$$f_h=\frac{\partial z}{\partial\tau}. \tag{12.52}$$

The microthermal potential, z, represents the thermal potential between a pair of interacting points. The temperature difference between the material points $\mathbf{x}'$ and $\mathbf{x}$ at any time is given by

$$\tau(\mathbf{x}', \mathbf{x}, t) = \Theta(\mathbf{x}', t) - \Theta(\mathbf{x}, t). \tag{12.53}$$

The thermal potential at point $\mathbf{x}$ is then a summation over all microthermal potentials associated with this point, and is defined as

$$Z(\mathbf{x}, t) = \frac{1}{2} \int_H z(\mathbf{x}', \mathbf{x}, t) dV_{\mathbf{x}'}. \tag{12.54}$$

The pairwise heat flow density function, f_h, can be expressed as

$$f_h(\mathbf{x}', \mathbf{x}, t) = \kappa \frac{\tau(\mathbf{x}', \mathbf{x}, t)}{|\boldsymbol{\xi}|}, \tag{12.55}$$

where κ is the thermal microconductivity. The microthermal potential corresponding to the thermal response function, f_h, can be obtained as

$$z = \kappa \frac{\tau^2}{2|\boldsymbol{\xi}|}. \tag{12.56}$$

The microconductivity is a PD parameter that can be related to the standard conductivity for a specified horizon.

12.8 Peridynamic Microconductivity

The microconductivity can be determined by equating the peridynamic thermal potential to the classical thermal potential at a point arising from a simple linear temperature field. The expression for the microconductivity will differ depending on the form of the thermal response function. The form given in Eq. 12.55 differs from those introduced by Bobaru and Duangpanya (2010, 2012) and Gerstle et al. (2008). In the most general case, heat transfer through a medium is three dimensional. However, certain problems can be classified as two or one dimensional depending on the relative magnitudes of heat transfer rates in different directions.

12.8.1 One-Dimensional Analysis

For one-dimensional analysis, a simple linear temperature field of the form $\Theta(x) = x$ results in the PD temperature difference of

$$\tau = \Theta(x') - \Theta(x) = x' - x = \xi = |\boldsymbol{\xi}|. \tag{12.57}$$

Invoking this temperature difference into Eq. 12.56 results in the PD microthermal potential as

$$z = \kappa \frac{\xi^2}{2|\boldsymbol{\xi}|}, \tag{12.58}$$

where $|\boldsymbol{\xi}| = |\mathbf{x}' - \mathbf{x}|$. Substituting for z from Eq. 12.58 into Eq. 12.54 and performing the integration leads to the PD thermal potential as

$$Z = \frac{1}{2}\int_H z(\xi) dV_{\boldsymbol{\xi}} = \frac{\kappa}{2}\int_0^{\delta}\left(\frac{\xi^2}{|\boldsymbol{\xi}|}\right) A d\xi = \frac{\kappa \delta^2 A}{4}, \tag{12.59}$$

where A is the cross-sectional area of the volume associated with the material point $\mathbf{x}'$. The corresponding classical thermal potential from Eq. 12.33b is obtained as

$$\hat{Z} = \frac{1}{2}k. \tag{12.60}$$

Equating the peridynamic thermal potential in Eq. 12.59 to the classical thermal potential given in Eq. 12.60 and solving for κ results in the PD microconductivity for one-dimensional analysis as

$$\kappa = \frac{2k}{A\delta^2}. \tag{12.61}$$

12.8.2 Two-Dimensional Analysis

For two-dimensional analysis, a simple linear temperature field of the form $\Theta(x, y) = (x + y)$ results in the PD temperature difference of

$$\tau = \Theta(x', y') - \Theta(x, y) = x' + y' \tag{12.62}$$

for the material point of interest, $\mathbf{x}$, located at the origin $(x = 0, y = 0)$. Invoking this temperature difference into Eq. 12.56 results in the PD microthermal potential as

$$z = \kappa \frac{(x' + y')^2}{2|\boldsymbol{\xi}|}, \tag{12.63}$$

where $|\boldsymbol{\xi}| = \sqrt{x'^2 + y'^2}$. Substituting for z from Eq. 12.63 into Eq. 12.54 and performing the integration over the horizon leads to the PD thermal potential as

$$Z(\mathbf{x}, t) = \frac{1}{2} \int_0^{2\pi} \int_0^{\delta} \kappa \frac{(\xi Cos(\theta) + \xi Sin(\theta))^2}{2|\boldsymbol{\xi}|} h \xi d\xi d\theta = \frac{\pi h \kappa \delta^3}{6}, \tag{12.64}$$

in which polar coordinates, (ξ, θ), are utilized to perform the integration over a disk with thickness h and radius δ. The corresponding classical thermal potential from Eq. 12.33b is obtained as

$$\hat{Z} = k. \tag{12.65}$$

Equating the PD thermal potential in Eq. 12.64 to the classical thermal potential given in Eq. 12.65 and solving for κ results in the PD microconductivity for two-dimensional analysis as

$$\kappa = \frac{6k}{\pi h \delta^3}. \tag{12.66}$$

12.8.3 Three-Dimensional Analysis

For three-dimensional analysis, a simple linear temperature field of the form $\Theta(x, y) = (x + y + z)$ results in the PD temperature difference of

$$\tau = \Theta(x', y', z') - \Theta(x, y, z) = (x' + y' + z') \tag{12.67}$$

for the material point of interest, $\mathbf{x}$, located at the origin $(x = 0, y = 0, z = 0)$. Invoking this temperature difference into Eq. 12.56 results in the PD microthermal potential as

$$z = \kappa \frac{(x' + y' + z')^2}{2|\boldsymbol{\xi}|}, \tag{12.68}$$

where $|\boldsymbol{\xi}| = \sqrt{x'^2 + y'^2 + z'^2}$. Substituting for z from Eq. 12.68 into Eq. 12.54 and performing the integration over the horizon leads to the PD thermal potential as

$$Z(\mathbf{x},t) = \frac{1}{2}\int_0^{\delta}\int_0^{2\pi}\int_0^{\pi}\kappa\frac{(\xi Cos(\theta)Sin(\phi)+\xi Sin(\theta)Sin(\phi)+\xi Cos(\phi))^2}{2|\boldsymbol{\xi}|} \times Sin\phi d\phi d\theta\xi^2 d\xi = \frac{\pi\kappa\delta^4}{4}, \tag{12.69}$$

in which spherical coordinates, (ξ,θ,ϕ), are utilized to perform the integration over a sphere with radius δ. The corresponding classical thermal potential from Eq. 12.33b is obtained as

$$\hat{Z} = \frac{3}{2}k. \tag{12.70}$$

Equating the peridynamic thermal potential in Eq. 12.69 to the classical thermal potential given in Eq. 12.70 and solving for κ results in the PD microconductivity for three-dimensional analysis as

$$\kappa = \frac{6k}{\pi\delta^4}. \tag{12.71}$$

12.9 Numerical Procedure

Numerical techniques are employed in order to solve for the PD thermal diffusion equation. The region of interest is discretized into subdomains in which the temperature is assumed to be constant. Thus, each subdomain is represented as a single integration point located at its mass center with an associated volume and integration weight, $w_{(j)} = 1$. Subsequently, the integration in the governing equation, given in Eq. 12.51, is numerically performed as

$$\rho_{(i)}c_{v(i)}\dot{\Theta}^n_{(i)} = \sum_{j=1}^{N} f_h\left(\boldsymbol{\tau}^n\left(\mathbf{x}_{(j)}-\mathbf{x}_{(i)}\right)\right)V_{(j)} + h^n_{s(i)}, \tag{12.72}$$

for which n is the time step number, i represents the point of interest, and j represents the points within the horizon of i. The volume of the subdomain associated with the collocation point $\mathbf{x}_{(j)}$ is denoted by $V_{(j)}$. The time integration is accomplished using the forward difference time stepping scheme. When forward differencing is employed, the following equation is solved:

$$\Theta_{(i)}^{n+1} = \Theta_{(i)}^{n} + \frac{\Delta t}{\rho_{(i)} c_{v(i)}} \left\{ \sum_{j=1}^{N} f_h\left(\tau^n\left(\mathbf{x}_{(j)} - \mathbf{x}_{(i)}\right)\right) V_{(j)} + h_{s(i)}^n \right\}, \tag{12.73}$$

where Δt is the time step size.

12.9.1 Discretization and Time Stepping

A one-dimensional region is considered to describe the details of the numerical scheme. The discretization of a one-dimensional region into subdomains is depicted in Fig. 12.5. Each subdomain has one integration point. The integration point represents a material point. The solution is constructed for material point $\mathbf{x}_{(i)}$. The material point $\mathbf{x}_{(i)}$ interacts with all points within its horizon, represented by $\mathbf{x}_{(j)}$. As shown in Fig. 12.6, material point $\mathbf{x}_{(i)}$ interacts with six other material points, $\mathbf{x}_{(j)}$ $(j = i-3,\ i-2,\ i-1,\ i+1,\ i+2,$ and $i+3)$, in its horizon. Thus, the radius of the horizon is $\delta = 3\Delta$, where $\Delta = |x_{(i+1)} - x_{(i)}|$.

The discretized form of the PD thermal diffusion equation for material point $\mathbf{x}_{(i)}$ becomes

$$\rho_{(i)} c_{v(i)} \dot{\Theta}_{(i)}^{n} = \sum_{j=1}^{N} f_{h(i)(j)}^{n} V_{(j)} + h_{s(i)}^{n}, \tag{12.74}$$

in which the thermal response function, represented by $f_{h(i)(j)}^{n}$, is determined at each time step for every interaction. The discretized equation for the thermal response function, f_h, is cast as

$$f_{h(i)(j)}^{n} = \kappa \frac{\tau_{(i)(j)}^{n}}{\left|\boldsymbol{\xi}_{(i)(j)}\right|}. \tag{12.75}$$

The relative initial position is defined as $\boldsymbol{\xi}_{(i)(j)} = \mathbf{x}_{(j)} - \mathbf{x}_{(i)}$ while the relative temperature is defined as $\tau_{(i)(j)}^{n} = \Theta_{(j)}^{n} - \Theta_{(i)}^{n}$. The thermal interaction of material point $\mathbf{x}_{(i)}$ with the points within its horizon is illustrated in Fig. 12.6.

The discretized thermal diffusion equation can be expanded as

$$\begin{aligned} \rho_{(i)} c_{v(i)} \dot{\Theta}_{(i)}^{n} = {} & f_{h(i)(i+1)}^{n} V_{(i+1)} + f_{h(i)(i+2)}^{n} V_{(i+2)} + f_{h(i)(i+3)}^{n} V_{(i+3)} \\ & + f_{h(i)(i-1)}^{n} V_{(i-1)} + f_{h(i)(i-2)}^{n} V_{(i-2)} + f_{h(i)(i-3)}^{n} V_{(i-3)} + h_{s(i)}^{n}. \end{aligned} \tag{12.76}$$

For marching in time, the forward differencing scheme is used. The time derivative of temperature at material point $\mathbf{x}_{(i)}$ is determined at the current time

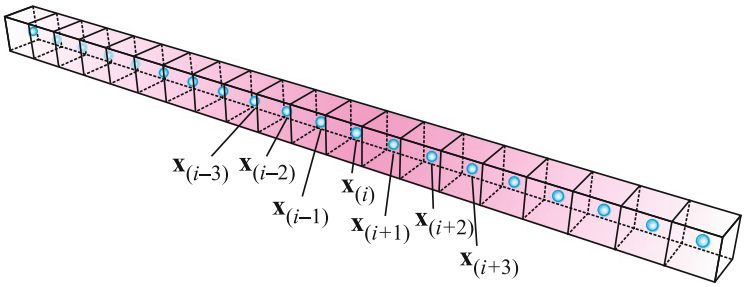

Fig. 12.5 Discretization of one-dimensional region with collocation points

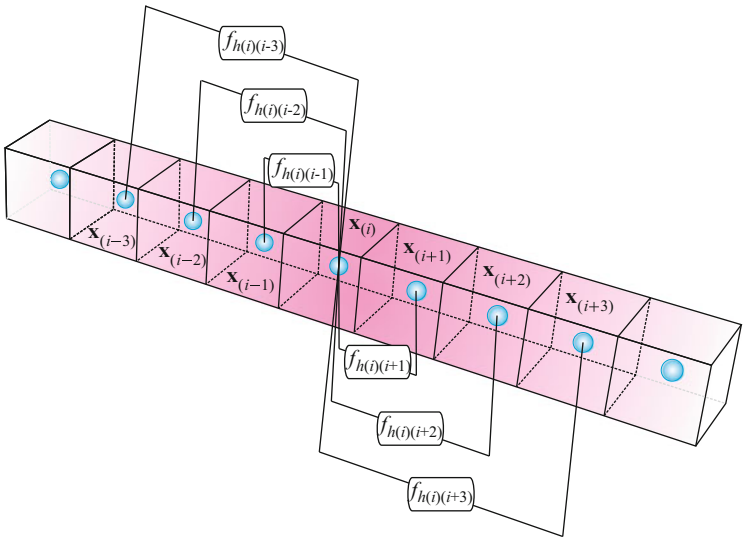

Fig. 12.6 Thermal interaction of points with the horizon of material point $\mathbf{x}_{(i)}$

step, n, from Eq. 12.76. By employing time integration via the forward differencing technique, the temperature at the next time step, $(n + 1)$, is determined. This algorithm may be expressed as

$$\Theta_{(i)}^{n+1} = \Theta_{(i)}^{n} + \Delta t \dot{\Theta}_{(i)}^{n}. \tag{12.77}$$

12.9.2 Numerical Stability

The forward differencing method utilized for the numerical time integration of the peridynamic thermal diffusion equation is conditionally stable. Therefore, it is

necessary to develop a stability condition that sets the restriction on the time step size in order to prevent an unbounded numerical solution. Similar to that performed by Silling and Askari (2005), a von Neumann stability analysis is adopted in the derivation of the stability condition. Therefore, the temperature field at each time step is assumed in the form

$$\Theta_{(i)}^{n} = \zeta^{n} e^{\Gamma i\sqrt{-1}}, \tag{12.78}$$

where Γ, representing the wavenumber, is a real and positive number and ζ is a complex number. The condition on the time step size ensures that the solution does not grow in an unbounded manner over time. In order for the solution to be bounded over time, the following expression must hold true:

$$|\zeta| \leq 1 \tag{12.79}$$

for every wavenumber Γ.

The discretized peridynamic thermal diffusion equation may be recast as

$$\rho_{(i)} c_{v(i)} \dot{\Theta}_{(i)}^{n} = \sum_{j=1}^{N} \frac{\kappa}{|\boldsymbol{\xi}_{(i)(j)}|} \left(\Theta_{(j)}^{n} - \Theta_{(i)}^{n}\right) V_{(j)} + h_{s}{}_{(i)}^{n}. \tag{12.80}$$

In the absence of a heat source due to volumetric heat generation, invoking Eq. 12.78 into Eq. 12.80 leads to

$$\frac{\rho_{(i)} c_{v(i)}}{\Delta t} \left(\zeta^{n+1} - \zeta^{n}\right) e^{\Gamma i\sqrt{-1}} = \sum_{j=1}^{N} \frac{\kappa}{|\boldsymbol{\xi}_{(i)(j)}|} \left(\zeta^{n} e^{\Gamma(j-i)\sqrt{-1}} - \zeta^{n}\right) e^{\Gamma i\sqrt{-1}} V_{(j)}. \tag{12.81}$$

Canceling out common terms reduces Eq. 12.81 to

$$\begin{aligned} \frac{\rho_{(i)} c_{v(i)}}{\Delta t} (\zeta - 1) &= \sum_{j=1}^{N} \frac{\kappa}{|\boldsymbol{\xi}_{(i)(j)}|} \left(e^{\Gamma(j-i)\sqrt{-1}} - 1\right) V_{(j)} \\ &= \sum_{j=1}^{N} \frac{\kappa}{|\boldsymbol{\xi}_{(i)(j)}|} (\cos \Gamma(j-i) - 1) V_{(j)} \ . \end{aligned} \tag{12.82}$$

This equation can be recast as

$$\frac{\rho_{(i)} c_{v(i)}}{\Delta t} (\zeta - 1) = -M_{\Gamma}, \tag{12.83}$$

in which M_{Γ} is defined by

$$M_\Gamma = \sum_{j=1}^{N} \frac{\kappa}{|\boldsymbol{\xi}_{(i)(j)}|}(1 - \cos\Gamma(j-i))V_{(j)}. \tag{12.84}$$

Solving for ζ in Eq. 12.83 gives

$$\zeta = 1 - \frac{\Delta t}{\rho_{(i)}c_{v(i)}}M_\Gamma. \tag{12.85}$$

Enforcing the condition $|\zeta| \leq 1$ results in the following constraint:

$$0 \leq \frac{\Delta t}{\rho_{(i)}c_{v(i)}}M_\Gamma \leq 2. \tag{12.86}$$

The restriction on the time step size is determined as

$$\Delta t < \frac{2\rho_{(i)}c_{v(i)}}{M_\Gamma}. \tag{12.87}$$

For the condition $|\zeta| \leq 1$ to be valid for all wavenumbers, Γ, Eq. 12.84 leads to the condition of

$$M_\Gamma \leq \sum_{j=1}^{N} 2\frac{\kappa}{|\boldsymbol{\xi}_{(i)(j)}|}V_{(j)}. \tag{12.88}$$

Substituting Eq. 12.88 into Eq. 12.87 leads to the stability condition as

$$\Delta t < \frac{\rho_{(i)}c_{v(i)}}{\sum_{j=1}^{N}\frac{\kappa}{|\boldsymbol{\xi}_{(i)(j)}|}V_{(j)}}. \tag{12.89}$$

Due to the dependence of κ on the horizon, the stability condition given in Eq. 12.89 is dependent on δ.

12.10 Surface Effects

The PD microconductivity parameter, κ, that appears in the thermal response function, f_h, is determined by computing the thermal potential of a material point whose horizon is completely embedded in the material. The value of this parameter depends on the domain of integration defined by the horizon. Therefore, the value of κ requires correction if the material point is close to free surfaces or material

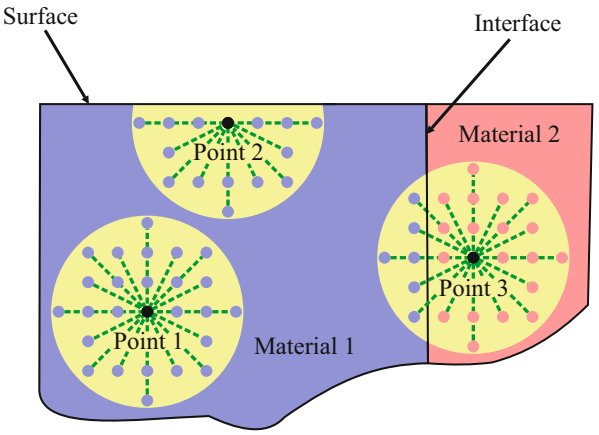

Fig. 12.7 Surface effects in the domain of interest

interfaces (Fig. 12.7). Since the presence of free surfaces is problem dependent, it is impractical to resolve this issue analytically. The correction of the material parameters is achieved by numerically integrating the PD thermal potential at each material point inside the body for simple temperature distribution and comparing it to its counterpart obtained from the classical thermal potential.

The simple temperature distribution can be linear in form, and the corresponding thermal potential, Z_∞, of a point completely embedded in the material is calculated using Eq. 12.33b. Subsequently, the PD thermal potential due to the applied linear temperature distribution is computed for each material point through numerical integration over its horizon from

$$Z_{(i)} = \frac{1}{2}\int_H z(\xi)dV_\xi = \frac{1}{2}\sum_{j=1}^{N} z_{(i)(j)}V_{(j)}, \tag{12.90}$$

in which the micropotential, $z_{(i)(j)}$, between material points $\mathbf{x}_{(i)}$ and $\mathbf{x}_{(j)}$ depends on the material microconductivity.

As shown in Fig. 12.8, the material point $\mathbf{x}_{(i)}$ may interact with material points $\mathbf{x}_{(j)}$ and $\mathbf{x}_{(m)}$. Material points $\mathbf{x}_{(i)}$ and $\mathbf{x}_{(j)}$ are embedded in material 1, and $\mathbf{x}_{(m)}$ is embedded in material 2. Thus, the microconductivity between points $\mathbf{x}_{(i)}$ and $\mathbf{x}_{(j)}$ is $\kappa_{(i)(j)}$, and it differs from $\kappa_{(i)(m)}$ between material points $\mathbf{x}_{(i)}$ and $\mathbf{x}_{(m)}$. Because the material points $\mathbf{x}_{(i)}$ and $\mathbf{x}_{(m)}$ are embedded in two different materials, their microconductivity, $\kappa_{(i)(m)}$, can be expressed in terms of an equivalent thermal conductivity as

$$k_{(i)(m)} = \frac{\ell_1 + \ell_2}{\frac{\ell_1}{k_1} + \frac{\ell_2}{k_2}}, \tag{12.91}$$

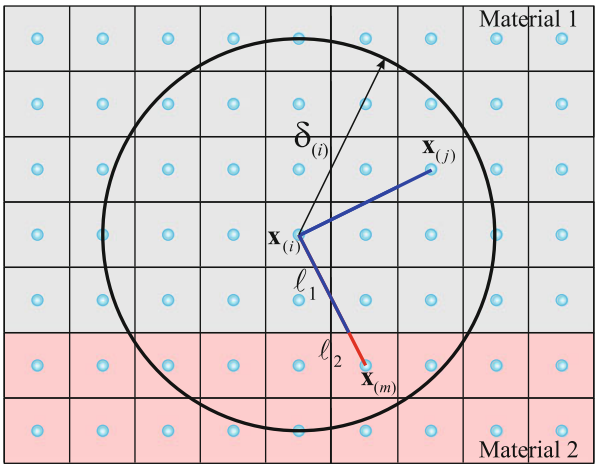

Fig. 12.8 Material point $\mathbf{x}_{(i)}$ close to an interface

in which ℓ_1 represents the segment of the distance between material points $\mathbf{x}_{(i)}$ and $\mathbf{x}_{(m)}$ in material 1 whose thermal conductivity is k_1, and ℓ_2 represents the segment in material 2 whose thermal conductivity is k_2.

The thermal potential of material point $\mathbf{x}_{(i)}$ is denoted by $Z_{(i)}$. The correction factor is determined for each material point in the domain as

$$g_{(i)} = \frac{Z_\infty}{Z_{(i)}}. \tag{12.92}$$

Therefore, the discretized thermal diffusion equation including the correction factor for point $\mathbf{x}_{(i)}$ becomes

$$\rho_{(i)} c_{v(i)} \dot{\Theta}^n_{(i)} = \sum_{j=1}^{N} g_{(i)(j)} f^n_{h(i)(j)} V_{(j)} + \rho_{(i)} s_b{}^n_{(i)}, \tag{12.93}$$

where $g_{(i)(j)} = g_{(i)} + g_{(j)}/2$. Finally, the discretized equation of motion for material point $\mathbf{x}_{(i)}$, including surface and volume correction, υ_c, is rewritten as

$$\rho_{(i)} c_{v(i)} \dot{\Theta}^n_{(i)} = \sum_{j=1}^{N} g_{(i)(j)} f^n_{h(i)(j)} \left(\upsilon_{c(j)} V_{(j)}\right) + \rho_{(i)} s_b{}^n_{(i)}. \tag{12.94}$$

Also, the thermal response functions between material points $\mathbf{x}_{(i)}$ and $\mathbf{x}_{(j)}$ and $\mathbf{x}_{(i)}$ and $\mathbf{x}_{(m)}$ are modified to reflect the change in microconductivity as

$$f^n_{h(i)(m)} = \kappa_{(i)(m)} \frac{\tau^n_{(i)(m)}}{\left|\boldsymbol{\xi}_{(i)(m)}\right|} \quad \text{and} \quad f^n_{h(i)(j)} = \kappa_{(i)(j)} \frac{\tau^n_{(i)(j)}}{\left|\boldsymbol{\xi}_{(i)(j)}\right|}. \tag{12.95}$$

12.11 Validation

In achieving the numerical results, the bond-based peridynamics approach is adopted while utilizing the numerical schemes described in the preceding sections. The predictions from the peridynamic simulations are compared against the classical solution to establish the validity of the peridynamic heat transfer analysis.

12.11.1 Finite Slab with Time-Dependent Surface Temperature

A finite slab initially at zero temperature is subjected to a boundary temperature that increases linearly with time. Its geometric description and discretization are depicted in Fig. 12.9.

Geometric Parameters

Slab thickness: $L = 0.01$ m

Material Properties

Specific heat capacity: $c_v = 64$ J/kgK
Thermal conductivity: $k = 233$ W/mK
Mass density: $\rho = 260\,\mathrm{kg/m^3}$

Initial Conditions

$\Theta(x, 0) = 0°\mathrm{C},\ 0 \leq x \leq L$

Boundary Conditions

$\Theta(0, t) = 0,\ \Theta(L, t) = At$ with $A = 500,\ 0 \leq t < \infty$

PD Discretization Parameters

Total number of material points in the x-direction: 100
Spacing between material points: $\Delta = 0.0001$ m

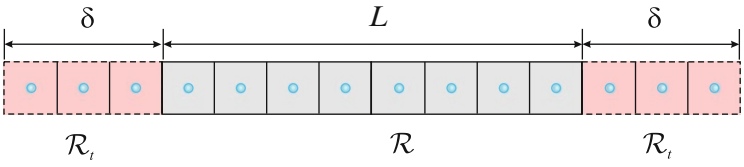

Fig. 12.9 Discretization of the finite slab and the fictitious boundary regions for temperatures

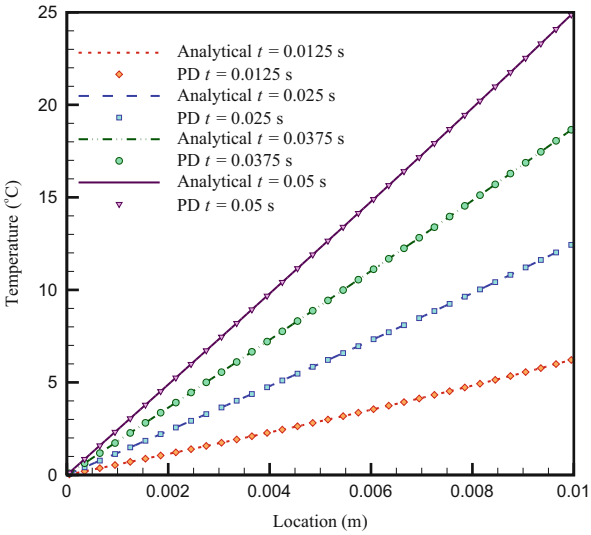

Fig. 12.10 Temperature variations from peridynamics and classical analytical solutions

Incremental volume of material points: $\Delta V = 1 \times 10^{-12}$ m^3
Volume of fictitious boundary layer: $V_\delta = (3) \times \Delta V = 3 \times 10^{-12}$ m^3
Horizon: $\delta = 3.015\Delta$
Time step size: $\Delta t = 10^{-6}$ s

The classical analytical solution (Jiji 2009) can be expressed as

$$\Theta(x,t) = A\frac{x}{L} + A\frac{\rho c_v 2L^2}{k\pi^3} \times \sum_{n=1}^{\infty} \frac{(-1)^n}{n^3} \sin\left(\frac{n\pi}{L}x\right)\left[1 - \exp\left(-\frac{k}{\rho c_v}\left(\frac{n\pi}{L}\right)^2 t\right)\right]. \tag{12.96}$$

The temperature variation is predicted at $t = 0.0125$ s, $t = 0.025$ s, $t = 0.0375$ s, and $t = 0.05$ s. Both analytical and PD predictions are shown in Fig. 12.10, and they are in close agreement. Because the temperature on the right boundary increases as a function of time, the rate of heat transfer from the right boundary also increases, as expected.

12.11.2 Slab with Convection Boundary Condition

A plate of thickness L, initially at temperature $\Theta(x,0) = F(x)$, dissipates heat by convection for times $t > 0$ from its surfaces into an environment at $\Theta_\infty = 0°\text{C}$. The plate initially has a linear temperature profile, and two surfaces are subjected

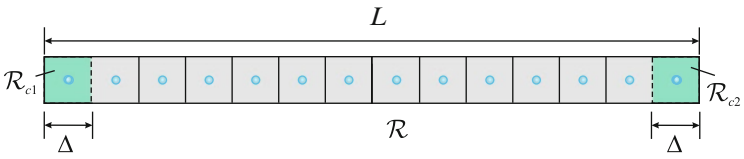

Fig. 12.11 Discretization of the finite slab and boundary regions for convection

to convective heat transfer. Its geometric description and discretization are depicted in Fig. 12.11.

Geometric Parameters

Slab thickness: $L = 1$ m

Material Properties

Specific heat capacity: $c_v = 64$ J/kgK
Thermal conductivity: $k = 233$ W/mK
Mass density: $\rho = 260\,\mathrm{kg/m^3}$

Initial Conditions

$\Theta(x,0) = F(x), \quad 0 \le x \le L, \;$ with $F(x) = x$

Boundary Conditions

$-k\partial\Theta/\partial x = h_1(\Theta_\infty - \Theta), \quad t > 0, \;$ at $x = 0$
$k\partial\Theta/\partial x = h_2(\Theta_\infty - \Theta), \quad t > 0, \;$ at $x = L$
with $h_1 = 10\,W/m^2K, \; h_2 = 20\,W/m^2K, \; \Theta_\infty = 0°\mathrm{C}$

PD Discretization Parameters

Total number of material points in the x-direction: 500
Spacing between material points: $\Delta = 0.002$ m
Incremental volume of material points: $\Delta V = 8 \times 10^{-9}$ m^3
Volume of boundary layer: $V_\Delta = 8 \times 10^{-9}$ m^3
Horizon: $\delta = 3.015\Delta$
Time step size: $\Delta t = 10^{-6}$ s
Rate of heat generation per unit volume at $x = 0$:
$h_{s1}(\mathbf{x},t) = h_1(\Theta_\infty - \Theta(\mathbf{x},t))/\Delta, \; \mathbf{x} \in \mathcal{R}_{c1}$
Rate of heat generation per unit volume at $x = L$:
$h_{s2}(\mathbf{x},t) = h_2(\Theta_\infty - \Theta(\mathbf{x},t))/\Delta, \; \mathbf{x} \in \mathcal{R}_{c2}$

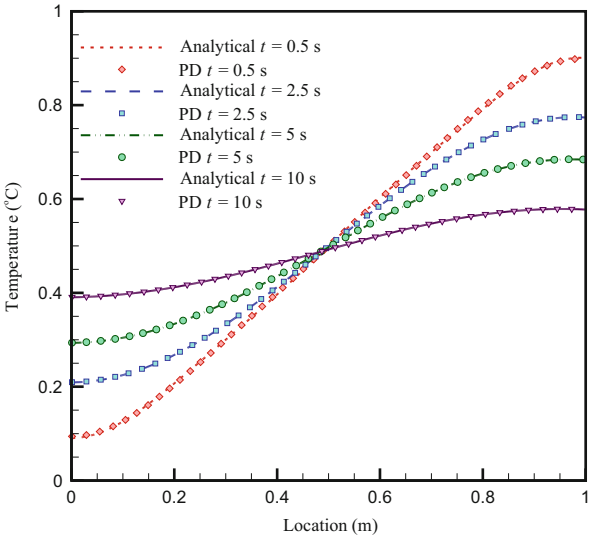

Fig. 12.12 Temperature variations from peridynamics and classical analytical solutions

The classical analytical solution of the problem is given by Özişik (1980) as

$$\Theta(x,t) = \sum_{m=1}^{\infty} e^{-\frac{k}{\rho c_v}\beta_m^2 t} \frac{1}{N(\beta_m)} X(\beta_m, x) \int_0^L X(\beta_m, x') F(x') dx', \tag{12.97}$$

in which $X(\beta_m, x)$ represents the eigenfunctions, β_m represents the eigenvalues, and $N(\beta_m)$ represents the normalization integral. The eigenfunctions, eigenvalues, and normalization integral are as follows:

$$X(\beta_m, x) = \beta_m Cos(\beta_m x) + H_1 Sin(\beta_m x), \tag{12.98a}$$

$$\tan(\beta_m L) = \frac{\beta_m (H_1 + H_2)}{\beta_m^2 - H_1 H_2}, \tag{12.98b}$$

$$N(\beta_m) = \frac{1}{2}\left[\left(\beta_m^2 + H_1^2\right)\left(L + \frac{H_2}{\beta_m^2 + H_2^2}\right) + H_1\right], \tag{12.98c}$$

with $H_1 = h_1/k$ and $H_2 = h_2/k$. The temperature variation is predicted at $t = 0.5$ s, $t = 2.5$ s, $t = 5$ s, and $t = 10$ s. Both analytical and PD predictions are shown in Fig. 12.12, and they are in close agreement.

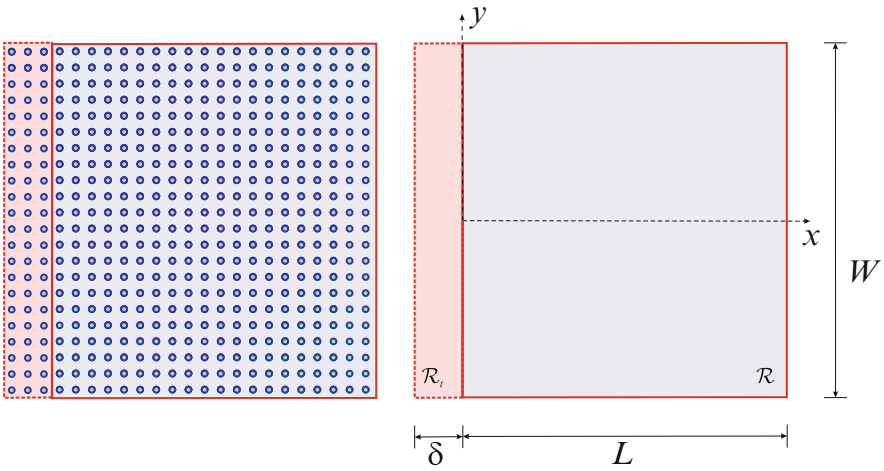

Fig. 12.13 Peridynamic model of the plate

12.11.3 Plate Under Thermal Shock with Insulated Boundaries

A square plate of isotropic material under thermal shock with insulated boundaries, shown in Fig. 12.13, was first considered by Hosseini-Tehrani and Eslami (2000) using the Boundary Element Method (BEM).

Geometric Parameters

Length: $L = 10$ m
Width: $W = 10$ m
Thickness: $H = 1$ m

Material Properties

Specific heat capacity: $c_v = 1$ J/kgK
Thermal conductivity: $k = 1$ W/mK
Mass density: $\rho = 1$ kg/m^3

Initial Conditions

$\Theta(x, y, t = 0) = 0°\text{C}$

Boundary Conditions

$\Theta_{,x}(x = 10, y) = 0, \quad t > 0$
$\Theta_{,y}(x, y = \pm 5) = 0, \quad t > 0$
$\Theta(x = 0, t) = 5te^{-2t}, \quad t > 0$

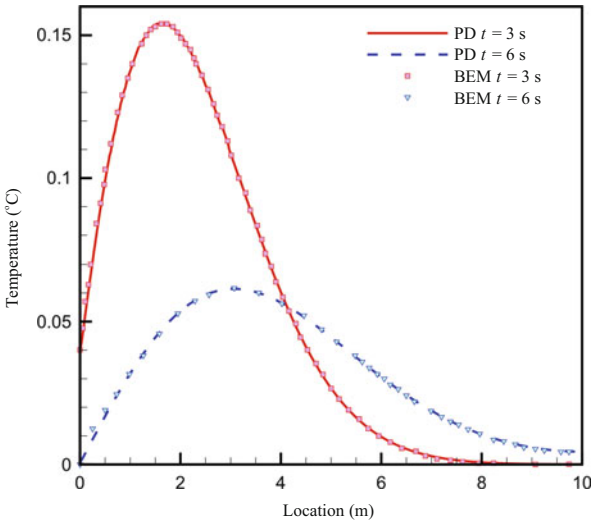

Fig. 12.14 Temperature variation from peridynamics and BEM at $y = 0$ (Hosseini-Tehrani and Eslami 2000)

PD Discretization Parameters

Total number of material points in the x-direction: 500
Total number of material points in the y-direction: 500
Spacing between material points: $\Delta = 0.02$ m
Incremental volume of material points: $\Delta V = 4 \times 10^{-4}\,\text{m}^3$
Volume of fictitious boundary layer: $V_\delta = (3 \times 500) \times \Delta V = 0.6\,\text{m}^3$
Horizon: $\delta = 3.015\Delta$
Time step size: $\Delta t = 5 \times 10^{-4}$ s

The temperature variations at $y = 0$ are predicted for $t = 3$ s and $t = 6$ s. Both BEM and PD predictions are shown in Fig. 12.14, and they are in close agreement.

12.11.4 Three-Dimensional Block with Temperature and Insulated Boundaries

A block of isotropic material is subjected to constant temperatures at both ends while its lateral surfaces are insulated. The schematic of the problem is described in Fig. 12.15.

Geometric Parameters

Length: $L = 0.01$ m
Width: $W = 0.001$ m
Thickness: $H = 0.001$ m

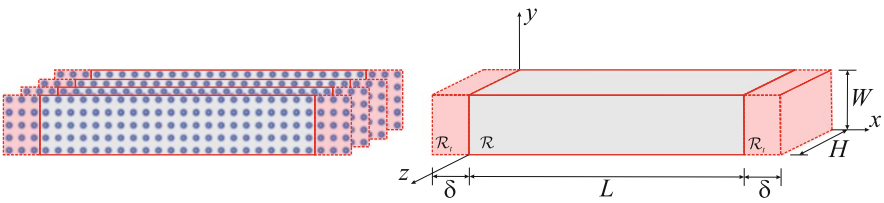

Fig. 12.15 Peridynamic model of a three-dimensional block

Material Properties

Specific heat capacity: $c_v = 64$ J/kgK
Thermal conductivity: $k = 233$ W/mK
Mass density: $\rho = 260$ kg/m^3

Initial Conditions

$$\Theta(x, y, z, 0) = 100°\text{C}, \quad 0 \le x \le L, \quad 0 \le y \le W, \quad 0 \le z \le H$$

Boundary Conditions

$$\Theta(0, y, z, t) = 0°\text{C}, \quad \Theta(L, y, z, t) = 300°\text{C}, \quad t > 0$$
$$\Theta_{,y}(x, 0, z, t) = 0, \quad \Theta_{,y}(x, W, z, t) = 0, \quad t > 0$$
$$\Theta_{,z}(x, y, 0, t) = 0, \quad \Theta_{,z}(x, y, H, t) = 0, \quad t > 0$$

PD Discretization Parameters

Total number of material points in the x-direction: 100
Total number of material points in the y-direction: 10
Total number of material points in the z-direction: 10
Spacing between material points: $\Delta = 0.0001$ m
Incremental volume of material points: $\Delta V = 1 \times 10^{-12}$ m^3
Volume of fictitious boundary layer: $V_\delta = (3 \times 10 \times 10) \times \Delta V = 3 \times 10^{-10}$ m^3
Horizon: $\delta = 3.015\Delta$
Time step size: $\Delta t = 10^{-7}$ s

Since the block is insulated on its lateral surfaces, the temperature profile along the block can be compared with the one-dimensional analytical solution of the problem given by

$$\Theta(x,t) = \Theta(0,t) - \frac{\Theta(0,t) - \Theta(L,t)}{L} x - \frac{2}{L} \sum_{n=1,3,5,\ldots}^{\infty} \sin\left(\frac{n\pi}{L} x\right) \times \left[\frac{L}{n\pi}\left(\Theta(0,t) - (-1)^n \Theta(L,t)\right) - \frac{100L}{n\pi}\left((-1)^n - 1\right)\right] e^{-\frac{k}{\rho c_v}\left(\frac{n^2\pi^2}{L^2}\right)t} . \tag{12.99}$$

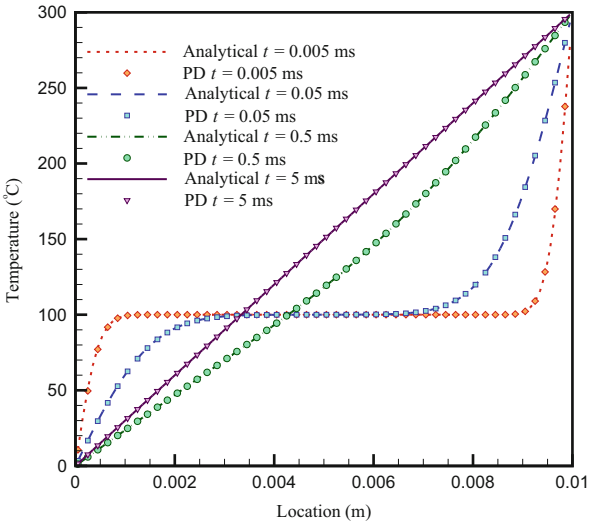

Fig. 12.16 Temperature variations from peridynamics and classical analytical solutions

The temperature variation is predicted at $t = 5 \times 10^{-6}$s, $t = 5 \times 10^{-5}$s, $t = 5 \times 10^{-4}$s, and $t = 5 \times 10^{-3}$s. As the block reaches a steady-state condition, the temperature profile approaches a linear variation along the block. As observed in Fig. 12.16, the thermal response predicted by the peridynamic heat transfer model is in close agreement with the analytical solution.

12.11.5 Dissimilar Materials with an Insulated Crack

In order to verify the peridynamic model in solving for the heat transfer concerning dissimilar materials, a plate with two different materials having an insulated interface crack is considered, as shown in Fig. 12.17. The peridynamic predictions and their comparison with ANSYS are given in Fig. 12.18. As observed, there is a close agreement.

Geometric Parameters

Length: $L = 2$ cm
Width : $W = 2$ cm
Thickness: $H = 0.01$ cm
Crack length: $2a = 1.0$ cm

Material Properties

Specific heat capacity: $c_v = 1$ J/kgK
Thermal conductivity: $k = 1.14$ W/cmK
Mass density: $\rho = 1\,\text{kg/cm}^3$

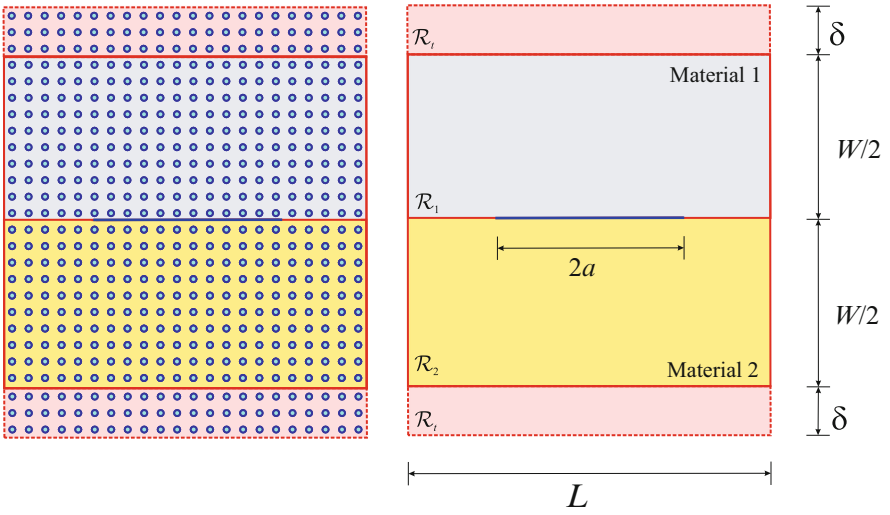

Fig. 12.17 Peridynamic model of a plate with an insulated interface crack

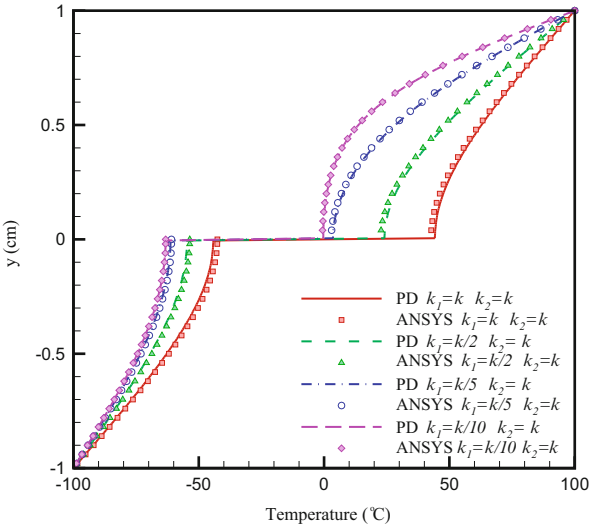

Fig. 12.18 Temperature variations along $x = 0$, across the interface of the plates with thermal conductivity k_1 for the upper half and k_2 for the lower half at $t = 0.5$ s

Initial Conditions

$$\Theta(x, y, z, 0) = 0, \quad -L/2 \le x \le L/2, \quad -W/2 \le y \le W/2$$

Boundary Conditions

$$\Theta(x, W/2, t) = 100^{\circ}\mathrm{C}, \quad \Theta(x, -W/2, t) = -100^{\circ}\mathrm{C}, \quad t > 0$$
$$\Theta_{,x}(L/2, y, t) = 0, \quad \Theta_{,x}(-L/2, y, t) = 0, \quad t > 0$$

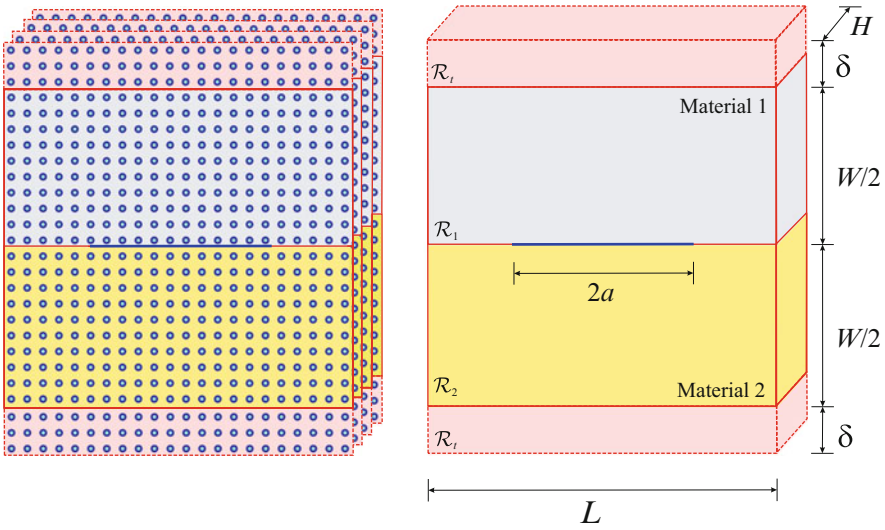

Fig. 12.19 Three-dimensional peridynamic model of a plate with a crack

PD Discretization Parameters

Total number of material points in the x-direction: 200
Total number of material points in the y-direction: 200
Spacing between material points: $\Delta = 0.01$ cm
Incremental volume of material points: $\Delta V = 1 \times 10^{-6}$ cm^3
Volume of fictitious boundary layer: $V_\delta = (3 \times 200) \times \Delta V = 6 \times 10^{-4}$cm^3
Horizon: $\delta = 3.015 \times \Delta$
Time step size: $\Delta t = 10^{-4}$ s

In order to demonstrate the three-dimensional capability of the PD analysis, the plate geometry with an insulated crack is also discretized in the thickness direction, as shown in Fig. 12.19. The peridynamic results are compared with the two-dimensional predictions. As observed in Fig. 12.20, there exists a close agreement between the two models.

Geometric Parameters

Length: $L = 2$ cm
Width: $W = 2$ cm
Thickness: $H = 0.2$ cm
Crack length: $2a = 1.0$ cm

Material Properties

Specific heat capacity: $c_v = 1$ J/kgK
Thermal conductivity: $k = 1.14$ W/cmK
Mass density: $\rho = 1\,\text{kg/cm}^3$

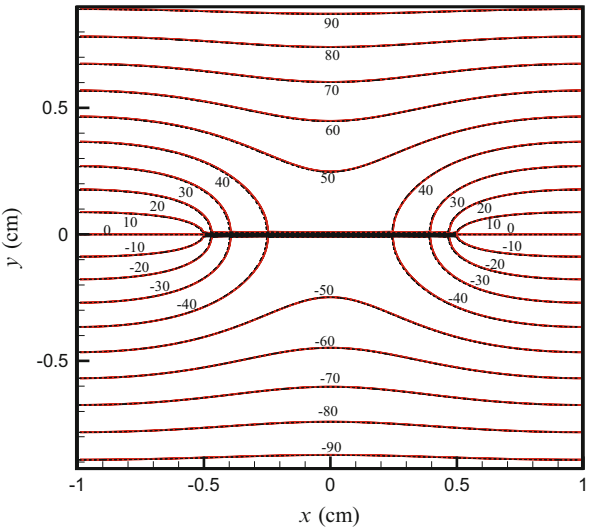

Fig. 12.20 Temperature field from two- and three-dimensional peridynamic analyses for $k_1 = k_2 = k$ at $t = 0.5$ s (two-dimensional model = *solid line*, three-dimensional model = *dashed line*)

Initial Conditions

$$\Theta(x, y, z, 0) = 0 - L/2 \le x \le L/2, \quad -W/2 \le y \le W/2, \quad -H \le z \le 0$$

Boundary Conditions

$$\Theta(x, W/2, z, t) = 100°\text{C}, \quad \Theta(x, -W/2, z, t) = -100°\text{C}, \quad t > 0$$
$$\Theta_{,x}(L/2, y, z, t) = 0, \quad \Theta_{,x}(-L/2, y, z, t) = 0, \quad t > 0$$
$$\Theta_{,z}(x, y, 0, t) = 0, \quad \Theta_{,z}(x, y, -H, t) = 0, \quad t > 0$$

PD Discretization Parameters

Total number of material points in the x-direction: 100
Total number of material points in the y-direction: 100
Total number of material points in the z-direction: 10
Spacing between material points: $\Delta = 0.02$ cm
Incremental volume of material points: $\Delta V = 8 \times 10^{-6}$ cm^3
Volume of fictitious boundary layer: $V_\delta = (3 \times 100 \times 10) \times \Delta V$ cm^3
Horizon: $\delta = 3.015 \times \Delta$
Time step size: $\Delta t = 10^{-5}$s

12.11.6 Thick Plate with Two Inclined Insulated Cracks

In order to further demonstrate the three-dimensional capability of the PD analysis, a thick plate with two insulated inclined cracks is considered under two different types of boundary conditions. The plate geometry is symmetric with respect to the

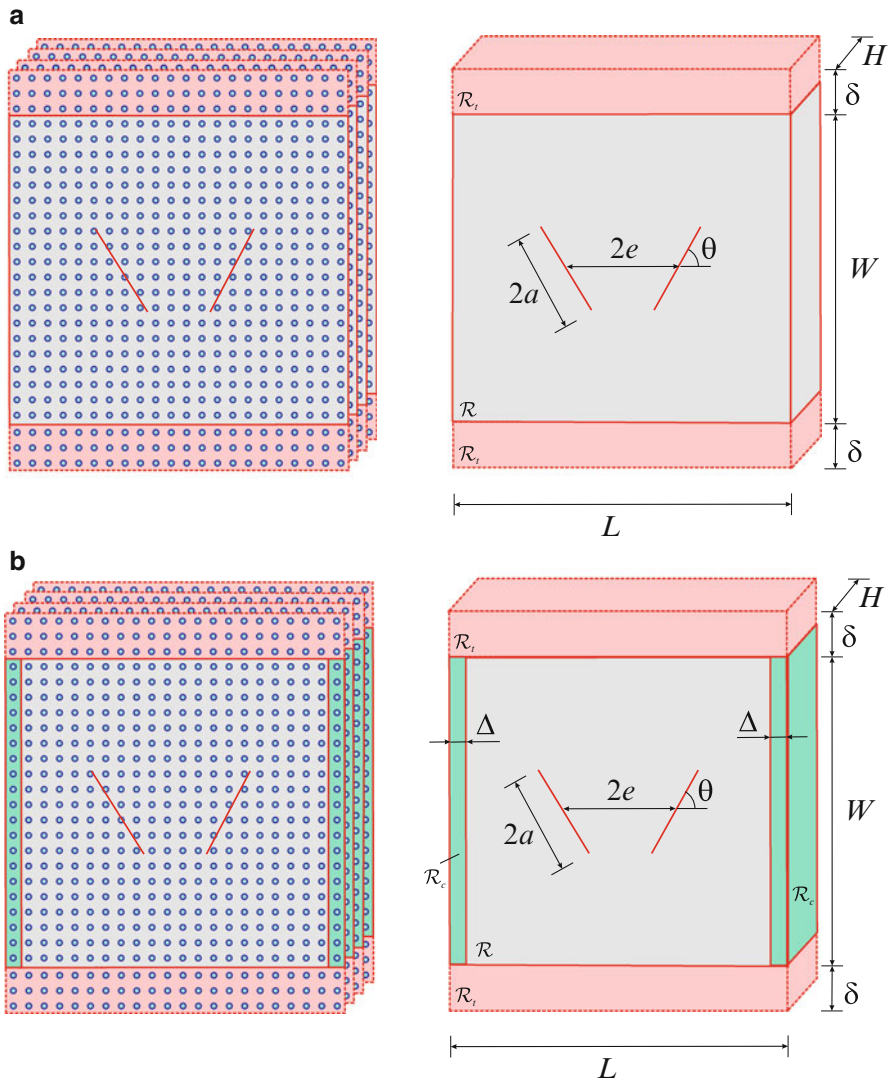

Fig. 12.21 Peridynamic model of the thick plate: (**a**) boundary conditions type I; (**b**) boundary conditions type-II

vertical direction. For the first type of boundary condition, the plate is subjected to constant temperature at the top and bottom surfaces while the remaining surfaces are insulated. For the second type of boundary condition, the plate is subjected to constant temperature at the top and bottom surfaces and convective heat transfer on the left and right surfaces while the remaining surfaces are insulated. The discretization and PD model of the plate for these two different types of boundary conditions are shown in Fig. 12.21a, b.

Geometric Parameters

Length: $L = 2$ cm
Width: $W = 2$ cm
Thickness: $H = 0.2$ cm
Crack lengths: $2a = 0.6$ cm
Crack orientations from horizontal direction: $\theta = 60^\circ$ and $\theta = 120^\circ$
Distance between crack centers: $2e = 0.66$ cm

Material Properties

Specific heat capacity: $c_v = 1\,\mathrm{J/kgK}$
Thermal conductivity: $k = 1.14\ \mathrm{W/cmK}$
Mass density: $\rho = 1\,\mathrm{kg/cm^3}$

Initial Conditions

$$\Theta(x, y, z, 0) = 0 \quad -L/2 \le x \le L/2, \quad -W/2 \le y \le W/2, \quad -H \le z \le 0$$

Boundary Conditions-I

$$\Theta(x, W/2, z, t) = 100^\circ\mathrm{C}, \quad \Theta(x, -W/2, z, t) = -100^\circ\mathrm{C}, \quad t > 0$$
$$\Theta_{,x}(L/2, y, z, t) = 0, \quad \Theta_{,x}(-L/2, y, z, t) = 0, \quad t > 0$$
$$\Theta_{,z}(x, y, 0, t) = 0, \quad \Theta_{,z}(x, y, -H, t) = 0, \quad t > 0$$

Boundary Conditions-II

$$\Theta(x, W/2, z, t) = 100^\circ\mathrm{C}, \quad \Theta(x, -W/2, z, t) = -100^\circ\mathrm{C}, \quad t > 0$$
$$-kT_{,x}(-L/2, y, z, t) = h(\Theta_\infty - \Theta), \quad t > 0$$
$$kT_{,x}(L/2, y, z, t) = h(\Theta_\infty - \Theta), \quad t > 0$$
$$h = 10\,\mathrm{W/cm^2K}, \quad \Theta_\infty = 0^\circ\mathrm{C}$$
$$\Theta_{,z}(x, y, 0, t) = 0, \quad \Theta_{,z}(x, y, -H, t) = 0, \quad t > 0$$

PD Discretization Parameters

Total number of material points in the x-direction: 100
Total number of material points in the y-direction: 100
Total number of material points in the z-direction: 10
Spacing between material points: $\Delta = 0.02$ cm
Incremental volume of material points: $\Delta V = 8 \times 10^{-6}\ \mathrm{cm}^3$
Volume of boundary layer: $V_\Delta = (1 \times 100 \times 10) \times \Delta V = 8 \times 10^{-3}\mathrm{cm}^3$
Volume of fictitious boundary layer: $V_\delta = (3 \times 100 \times 10) \times \Delta V = 24 \times 10^{-3}\mathrm{cm}^3$
Horizon: $\delta = 3.015 \times \Delta$
Time step size: $\Delta t = 10^{-5}\mathrm{s}$
Rate of heat generation per unit volume at $x = -L/2$ and $x = L/2$:
$h_s(\mathbf{x}, t) = \frac{1}{\Delta} h(\Theta_\infty - \Theta(\mathbf{x}, t)), \ \mathbf{x} \in \mathcal{R}_c$

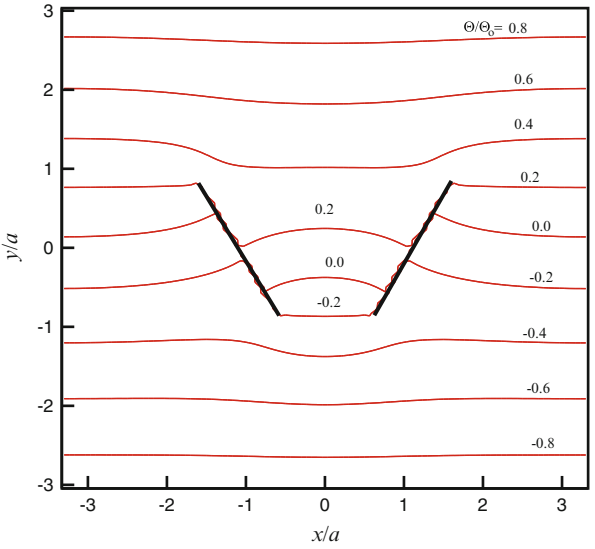

Fig. 12.22 Three-dimensional peridynamic temperature predictions on the mid-plane with a normal in the $+z$ direction at $t = 0.45$ s for boundary conditions type-I ($\Theta_0 = 100°\text{C}$)

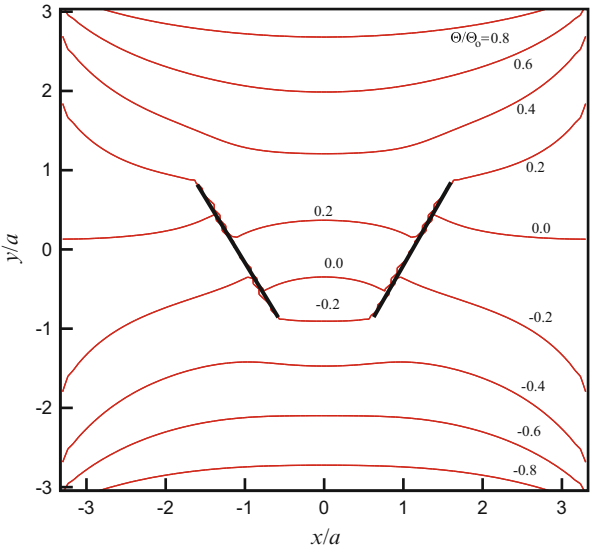

Fig. 12.23 Three-dimensional peridynamic temperature predictions on the mid-plane with a normal in the $+z$ direction at $t = 0.45$ s for boundary conditions type-II ($\Theta_0 = 100°\text{C}$)

For the first type of boundary condition, the peridynamic prediction for the temperature field is shown in Fig. 12.22. They are in close agreement with the classical solution (Chang and Ma 2001; Chen and Chang 1994). For the second type of boundary condition, the peridynamic prediction for the temperature field is shown in Fig. 12.23. For this case, there exists no classical solution for comparison.

References

Agwai A (2011) A peridynamic approach for coupled fields. Dissertation, University of Arizona
Alvarez FX, Jou D (2007) Memory and nonlocal effects in heat transport: from diffusive to ballistic regimes. Appl Phys Lett 90:083109
Bathe K (1996) Finite element procedures. Prentice Hall, Englewood Cliffs
Bobaru F, Duangpanya M (2010) The peridynamic formulation for transient heat conduction. Int J Heat Mass Transf 53:4047–4059
Bobaru F, Duangpanya M (2012) The peridynamic formulation for transient heat conduction in bodies with discontinuities. Int J Comp Phys 231:2764–2785
Chang CY, Ma CC (2001) Transient thermal conduction analysis of a rectangular plate with multiple insulated cracks by the alternating method. Int J Heat Mass Transf 44:2423–2437
Chen G (2002) Ballistic-diffusive equations for transient heat conduction from nano to macroscales. Trans ASME J Heat Transf 124:320–328
Chen WH, Chang CL (1994) Heat conduction analysis of a plate with multiple insulated cracks by the finite element alternating method. Int J Solids Struct 3:1343–1355
Dorfman AS (2004) Transient heat transfer between a semi-infinite hot plate and a flowing cooling liquid film. Trans ASME J Heat Transf 126:149–154
Duffey RB, Porthous D (1973) Physics of rewetting in water reactor emergency core cooling. Nucl Eng Des 25:379–394
Gerstle W, Silling S, Read D, Tewary V, Lehoucq R (2008) Peridynamic simulation of electromigration. Comput Mater Continua 8:75–92
Grmela M, Lebon G (1998) Finite-speed propagation of heat: a nonlocal and nonlinear approach. Physica A 248:428–441
Hosseini-Tehrani P, Eslami MR (2000) BEM analysis of thermal and mechanical shock in a two-dimensional finite domain considering coupled thermoelasticity. Eng Anal Bound Elem 24:249–257
Jiji ML (2009) Heat conduction. Springer, Berlin/Heidelberg
Lebon G, Grmela M (1996) Weakly nonlocal heat conduction in rigid solids. Phys Lett A 214:184–188
Luciani JF, Mora P, Virmont J (1983) Nonlocal heat-transport due to steep temperature-gradients. Phys Rev Lett 51:1664–1667
Mahan GD, Claro F (1988) Nonlocal theory of thermal-conductivity. Phys Rev B 38:1963–1969
Moiseiwitsch BL (2004) Variational principles. Dover, Mineola
Özişik MN (1980) Heat conduction, 2nd edn. Wiley, New York
Silling SA, Askari E (2005) A meshfree method based on the peridynamic model of solid mechanics. Comput Struct 83:1526–1535
Sobolev SL (1994) Equations of transfer in nonlocal media. Int J Heat Mass Transf 37:2175–2182
Tien CL, Chen G (1994) Challenges in microscale conductive and radiative heat-transfer. Trans ASME J Heat Transf 116:799–807
Tzou DY, Guo Z (2010) Non local behavior in thermal lagging. Int J Therm Sci 49:1133–1137